Published OnlineFirst on January 6, 2012; DOI:10.1158/1541-7786.MCR-11-0347

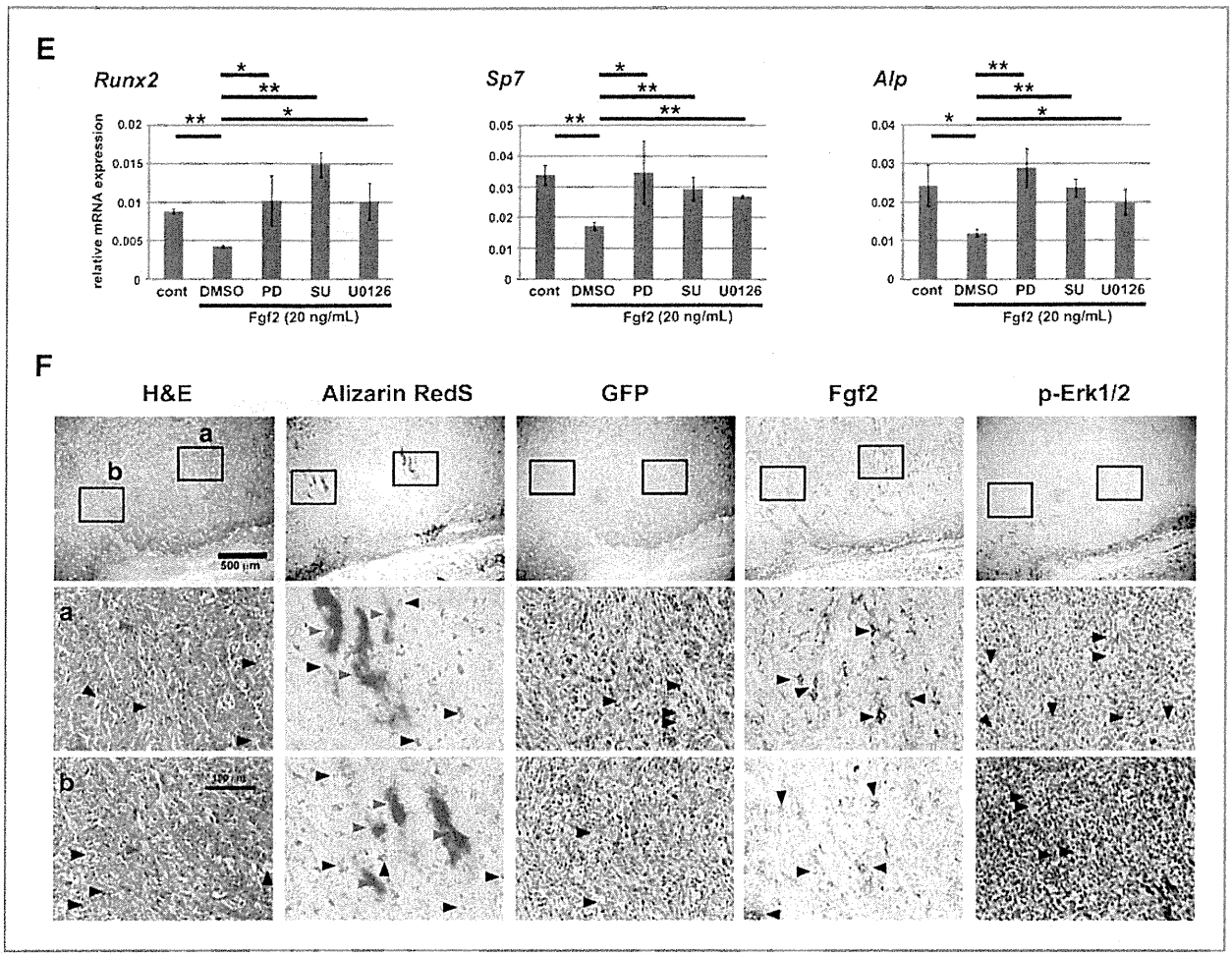

Figure 6. (*Continued*) E, AX cells were cultured in osteogenic medium supplemented with or without Fgf2 (20 ng/mL), SU5402 (SU, Fgfr inhibitor, 10 μg/mL), PD173074 (PD, Fgfr inhibitor, 1 μmol/L), or U0126 (Mek inhibitor, 50 μmol/L) for 1 day. The expression of osteogenic genes was assessed by real-time RT-PCR analysis. Results are shown as the ratio of the abundance of each mRNA to that of *Gapdh*. ($n = 3$). *, $P < 0.05$; **, $P < 0.005$ (the Student *t* test). F, immunohistochemistry of serial sections of an AX-derived osteosarcoma tumor. Black arrowheads and red arrowheads indicate the locations of Fgf2 polyhedra and osteogenic differentiation, respectively. Boxed regions are shown at a higher magnification in the bottom.

sensitivity to anticancer drugs in addition to maintaining immaturity in osteosarcoma cells.

Discussion

The histopathology of osteosarcoma includes a complex mixture of immature tumor cells and mature bone formation (3). It remains to be elucidated how these complicated structures are generated during osteosarcoma progression. The present study focused on the role of soluble factors such as Fgf2 and Lif released from nontumor cells in the osteosarcoma microenvironment.

Although the roles of Fgf2 or Lif on osteogenic differentiation are complicated and have not been fully clarified yet, both factors seem to possess similar potential for osteogenesis. The targeted disruption of each signaling pathway in mice resulted in a significant reduction in bone mass (28–30). In contrast, transgenic mice of Fgf2 exhibited a reduction in osteoblast differentiation and abnormal bone formation (31, 32). Fgf2 has also been found to promote proliferation and differentiation in osteoblasts and to increase bone formation (33–35). However, sustained exposure to a high concentration of Fgf2 inhibited osteogenesis by suppressing the production of bone materials (36–38). Similarly, Lif stimulated bone formation during the early proliferative stages of osteogenic process but inhibited it at later stages in osteoblast culture systems *in vitro* (39). Thus, both factors seem to show opposite impacts on osteoblast proliferation or differentiation at distinct stages of maturation, and the nonphysiologic exposure to both factors might result in the inhibition of osteogenesis (37, 39). AX cells are believed to have originated from transformed osteochondral progenitor cells (12). We suggest that Fgf2 and Lif mainly exert effects on proliferation and osteogenic suppression in AX cells in which the apoptotic program has been fully disrupted.

Published OnlineFirst on January 6, 2012; DOI:10.1158/1541-7786.MCR-11-0347

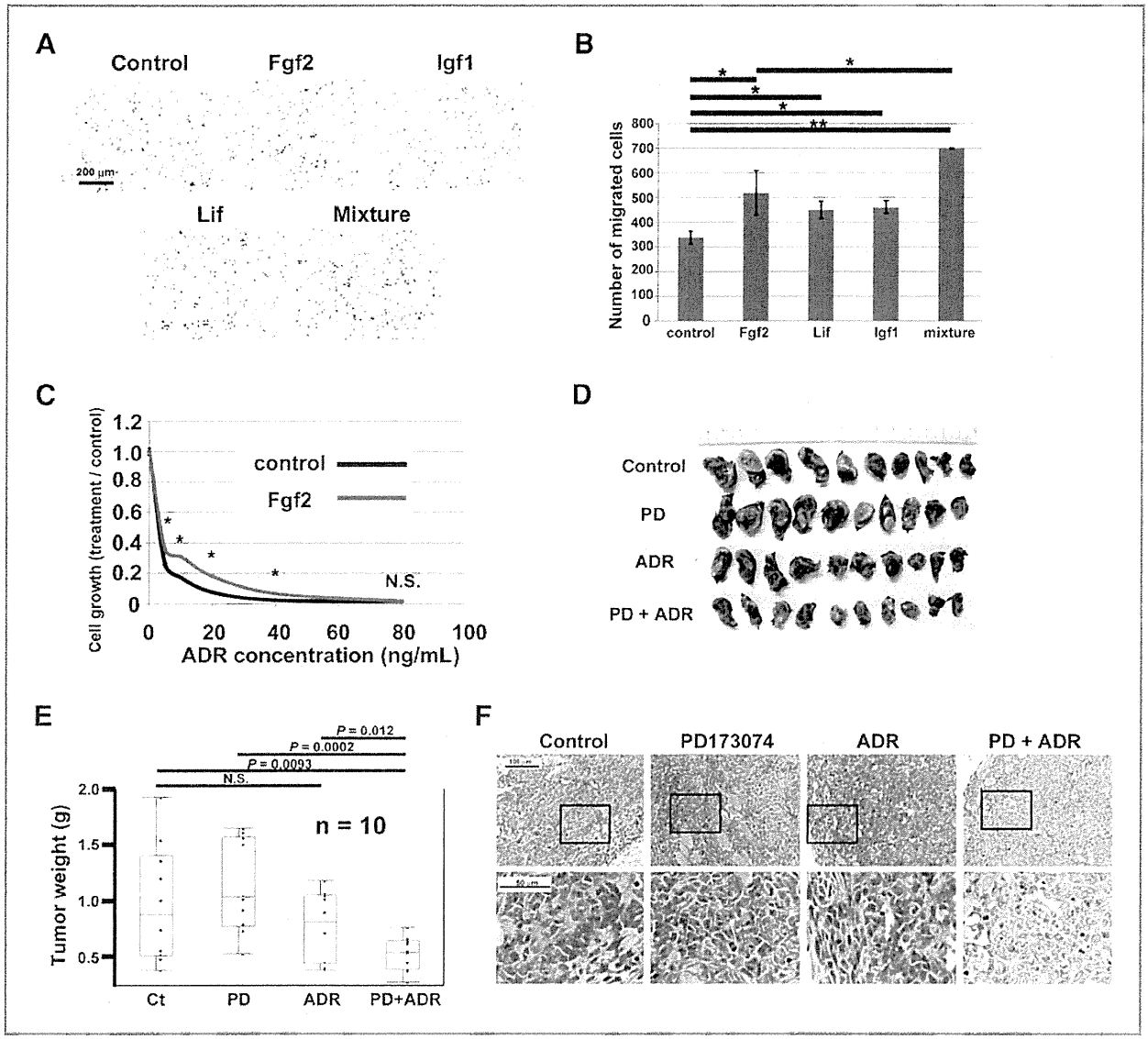

Figure 7. Fgf2 enhanced migration of osteosarcoma cells and afforded chemoresistance. A, the microscopic findings of migrated AX cells through Transwell membranes. B, migrated cells were counted and data are represented as means ± SD from 3 independent experiments. *, $P < 0.05$; **, $P < 0.001$ (the Student *t* test). C, cell proliferation of AX cells 2 days after treatment with Adriamycin (ADR) at the indicated concentrations was analyzed in the presence or absence of Fgf2 (20 ng/mL). Data are shown as the ratio of the measurement in the presence of each concentration of Adriamycin to that in the absence of Adriamycin and represented as means ± SDs from 3 independent experiments. *, $P < 0.05$; NS, not significant (the Student *t* test). D, a macroscopic finding of osteosarcoma tumors developed in mice with or without PD and/or Adriamycin treatment. E, tumor weight of AX-derived tumors developed in mice treated with or without PD and/or Adriamycin. F, immunohistochemistry of AX-derived osteosarcoma tumors in mice treated with each drug. Boxed regions are shown at a higher magnification in the bottom.

The physiologic roles of Erk activation in osteoblast differentiation also remain controversial and contradictory results have been observed, depending on the differential cell context or cell culture systems (40–42). A recent report showed that the cellular kinase activity of Erk1/2 was significantly downregulated during the differentiation of MC-3T3-E1 osteoblasts cultured for 7 days in the presence of ascorbic acid and β-glycerophosphate, which we used in our osteogenic culture system (43). Importantly, although both Fgf2 and Lif highly activated Erk1/2 in AX cells, the level of activation was more potent upon treatment with Fgf2 than with Lif (Fig. 3A). The suppression of osteogenic differentiation by Lif in AX cells was rescued by the Mek inhibitor PD98059 at 50 nmol/L, which was not able to restore the osteogenic ability inhibited by Fgf2 (Fig. 6D). Importantly, the restoration of osteogenesis suppressed by Lif treatment was also observed with another Mek inhibitor: U0126 at a lower concentration than that required for restoration in Fgf2 treatment (Fig. 6D). Moreover, Erk1/2 was more weakly phosphorylated by Igf1 than Fgf2

Published OnlineFirst on January 6, 2012; DOI:10.1158/1541-7786.MCR-11-0347

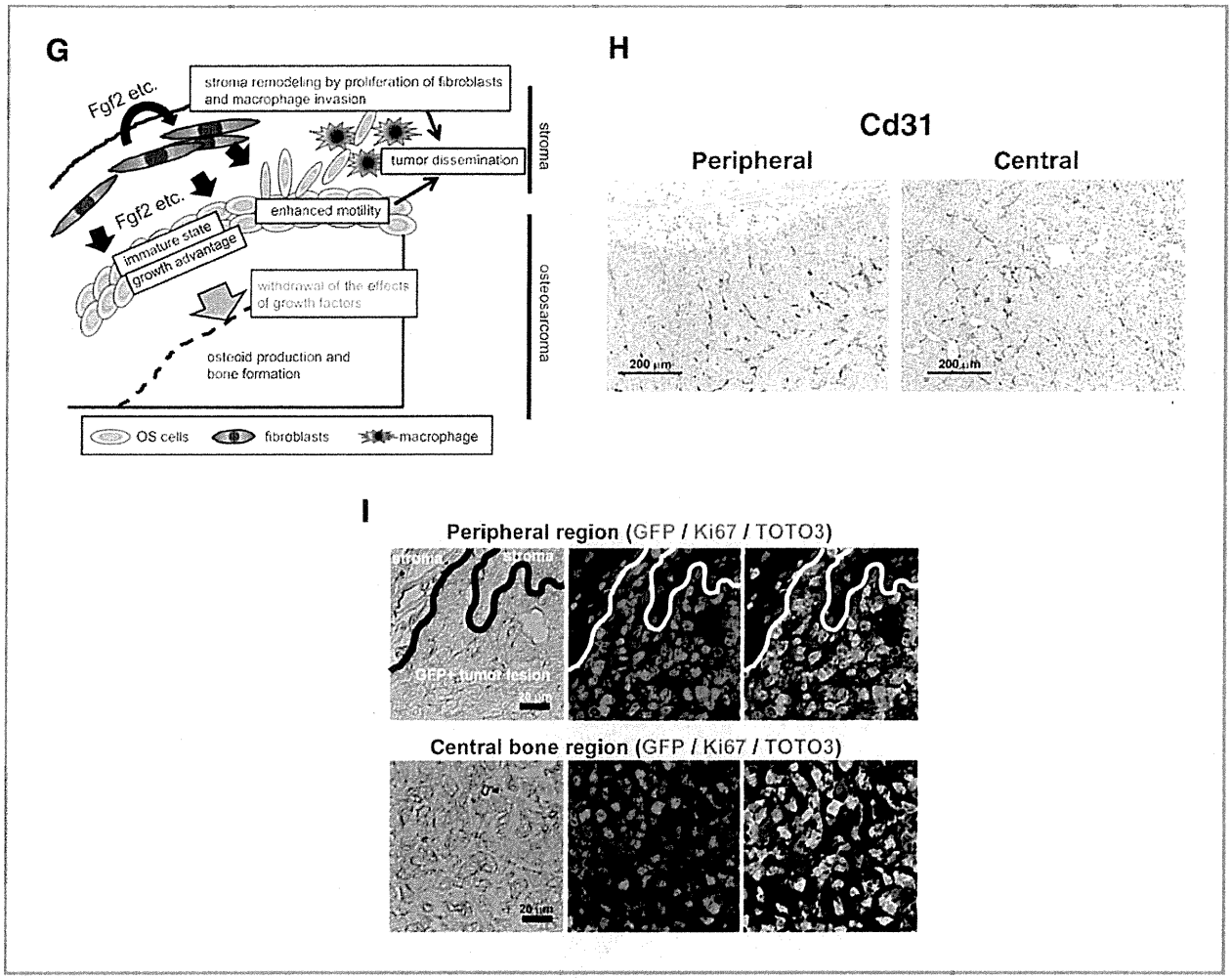

Figure 7. (*Continued*) G, the proposed model for osteosarcoma progression. Microenvironmental stromal cells release factors such as Fgf2, which maintain the immature state of osteosarcoma cells. Osteosarcoma cells inside the tumor exhibit osteogenesis accompanied by the withdrawal of the effects of environmental factors. In addition, these factors can enhance proliferation and motility of osteosarcoma cells. Stroma remodeling by the proliferation of fibroblasts and invasion of macrophages supports the dissemination of osteosarcoma cells. H, immunohistochemistry of an AX-derived osteosarcoma tumor for CD31. Both, a peripheral and an intratumor central region are shown. I, immunofluorescence analysis of Ki-67 expression in the peripheral or central part of an AX-derived osteosarcoma tumor. Tumor cells were identified by GFP staining. TOTO3 was used for nuclear staining.

or Lif, and the high concentration of Igf1 also blocked osteogenic activity (Fig. 2C). Also importantly, osteogenic differentiation of AX cells occurs in the areas where Erk1/2 activation was absent *in vivo* (Fig. 6F; Supplementary Fig. S4B). Collectively, these findings suggested that the suppression of osteogenesis in AX cells might be dependent on the strength of activation of Erk1/2.

Fgf2 mediates various cellular events and promotes tumor progression (20, 44, 45). It is also suggested to involve in differentiation and/or cell death in some tumors such as Ewing tumor (46, 47). Our results indicated that Fgf2 enhanced cellular proliferation and motility in AX cells (Figs. 2B and 7A and B). Importantly, Fgfr1 was highly expressed not only in tumor cells but also in stromal fibroblasts (Fig. 4B and C). In addition, nontumor fibroblastic cells clustered in the Fgf2 enriched areas generated by Fgf2 polyhedra (Supplementary Fig. S4A). It is possible that Fgf2 released from stromal fibroblasts enhances proliferation and motility in the fibroblasts themselves as well as tumor cells. Although further evaluation will be needed, such a positive feedback loop in tumor stromal cells mediated by Fgf2 might contribute to remodeling tumor surroundings into suitable environments for tumor progression (Fig. 7G). Angiogenesis is one of the important roles of Fgf2 in tumor progression (20, 48, 49). In our established osteosarcoma tumors, tumor vasculatures were equally abundant both in peripheral and inside regions (Fig. 7H). In fact, AX cells produce Vegfa (data not shown) and the concentration measured using tumor homogenate was high [4132.4 ± 1438.1 pg/mL (n = 3)]. Therefore, the role of Fgf2 in angiogenesis in our established model might be limited.

We wonder whether the enhancement of osteogenesis by withdrawal of each environmental factor alone could contribute to osteosarcoma cell death, resulting in an effective

Published OnlineFirst on January 6, 2012; DOI:10.1158/1541-7786.MCR-11-0347

therapeutic approach. Terminal differentiation accompanied by apoptosis is known to control osteoblast life span and bone formation (50). However, osteosarcoma cells appear to lapse into a differentiation block and AX cells may possibly return to an immature state from an osteogenic phase in the presence of Fgf2 (Fig. 4D). Consistent with this notion, a significant portion of osteosarcoma cells exhibited Ki-67 positivity, which is a marker for proliferative activity, in the region of bone formation in addition to the peripheral region of tumors (Fig. 7I). In view of therapeutic approaches to osteosarcoma, modulation of sensitivity to anticancer agents by Fgf2 might be more important (Fig. 7C, D, and E). Fgf2 might contribute to the formation of chemoresistant areas inside the tumors, resulting in residual disease *in vivo*.

Finally, some tumor malignant phenotypes such as cellular proliferation and motility were more enhanced by the mixture of several environmental factors than Fgf2 alone (Figs. 2B and 7B). Therefore, the combined blockade of signaling pathways of several growth factors, including Fgf2, may be useful in controlling the aggressiveness of osteosarcoma.

Disclosure of Potential Conflicts of Interest

No potential conflicts of interest were disclosed.

Acknowledgments

The authors thank I. Ishimatsu, T. Suzuki, and S. Hyashi for technical assistance and K. Arai for secretarial assistance.

Grant Support

This work was partly supported by grants from the Ministry of Education, Science, Sports, and Culture of Japan (to T. Shimizu and H. Saya) and a grant from the National Institute of Biomedical Innovation, Japan (to H. Saya).

The costs of publication of this article were defrayed in part by the payment of page charges. This article must therefore be hereby marked *advertisement* in accordance with 18 U.S.C. Section 1734 solely to indicate this fact.

Received July 21, 2011; revised November 29, 2011; accepted December 19, 2011; published OnlineFirst January 6, 2012.

References

1. Bielack SS, Kempf-Bielack B, Delling G, Exner GU, Flege S, Helmke K, et al. Prognostic factors in high-grade osteosarcoma of the extremities or trunk: an analysis of 1,702 patients treated on neoadjuvant cooperative osteosarcoma study group protocols. J Clin Oncol 2002; 20:776–90.
2. Clark JCM, Dass CR. A review of clinical and molecular prognostic factors in osteosarcoma. J Cancer Res Clin Oncol 2008;134: 281–97.
3. Fletcher CDM, Unni KK, Mertens F, editors. Osteogenic tumours: WHO classification tumours of soft tissue and bone. Lyon, France:IARC Press; 2002.
4. Gazdar AF, Kadoyama C, Venzon D, Park JG, Tsai CM, Linnoila RI, et al. Association between histological type and neuroendocrine differentiation on drug sensitivity of lung cancer cell lines. J Natl Cancer Inst Monogr 1992;13:191–6.
5. Silverberg SG. Histologic grading of ovarian carcinoma: a review and proposal. Int J Gynecol Pathol 2000;19:7–15.
6. Sethi T, Rintoul RC, Moore SM, MacKinnon AC, Salter D, Choo C, et al. Extracellular matrix proteins protect small cell lung cancer cells against apoptosis: a mechanism for small cell lung cancer growth and drug resistance *in vivo*. Nat Med 1999;5:662–8.
7. Uhm JH, Dooley NP, Kyritsis AP, Rao JS, Gladson CL. Vitronectin, a glioma-derived extracellular matrix protein, protects tumor cells from apoptotic death. Clin Cancer Res 1999;5:1587–94.
8. McAllister SS, Weinberg RA. Tumor-host interactions: a far-reaching relationship. J Clin Oncol 2010;28:4022–8.
9. Bissell MJ, Radisky D. Putting tumors in context. Nat Rev Cancer 2001;1:46–54.
10. DeWever O, Demetter P, Mareel M, Bracke M. Stromal myofibroblasts are drivers of invasive cancer growth. Int J Cancer 2008;123:2229–38.
11. Seruga B, Zhang H, Bernatein LJ, Tannock IF. Cytokines and their relationship to the symptoms and outcome of cancer. Nat Rev Cancer 2008;8:887–99.
12. Shimizu T, Ishikawa T, Sugihara E, Kuninaka S, Miyamoto T, Mabuchi Y, et al. c-MYC overexpression with loss of Ink4a/Arf transforms bone marrow stromal cells into osteosarcoma accompanied by loss of adipogenesis. Oncogene 2010;29:5687–99.
13. Ijiri H, Coulibaly F, Nishimura G, Nakai D, Chiu E, Takenaka C, et al. Structure-based targeting of bioactive proteins into cypovirus polyhedra and application to immobilized cytokines for mammalian cell culture. Biomaterials 2009;30:4297–308.
14. Mori H, Shukunami C, Furuyama A, Notsu H, Nishizaki Y, Hiraki Y. Immobilization of bioactive fibroblast growth factor-2 into cubic proteinous microcrystals (bombyx mori cypovirus polyhedra) that are insoluble in a physiological cellular environment. J Biol Chem 2007;282:17289–96.
15. Nishishita N, Ijiri H, Takenaka C, Kobayashi K, Goto K, Kotani E, et al. The use of leukemia inhibitory factor immobilized on virus-derived polyhedra to support the proliferation of mouse embryonic and induced pluripotent stem cells. Biomaterials 2011;32:3555–63.
16. Kubota Y, Takubo K, Shimizu T, Ohno H, Kishi K, Shibuya M, et al. M-CSF inhibition selectively targets pathological angiogenesis and lymphangiogenesis. J Exp Med 2009;206:1089–102.
17. Noonan DM, Barbaro ADL, Vannini N, Mortara L, Albini A. Inflammation, inflammatory cells and angiogenesis: decisions and indecisions. Cancer Metastasis Rev 2008;27:31–40.
18. Holmes C, Stanford WL. Stem cell antigen-1: expression, function, and enigma. Stem Cells 2007;25:1339–47.
19. Toma JG, Akhavan M, Fernandes KJL, Barnabe-Heider F, Sadikot A, Kaplan DR, et al. Isolation of multipotent adult stem cells from the dermis of mammalian skin. Nat Cell Biol 2001;3:778–84.
20. Turner N, Grose R. Fibroblast growth factor signaling: from development to cancer. Nat Rev Cancer 2010;10:116–29.
21. Heinrich PC, Behrmann I, Haan S, Hermanns HM, Muller-Newen G, Schanper F. Principles of interleukin (IL)-6-type cytokine signaling and its regulation. Biochem J 2003;374:1–20.
22. Rikhof B, de Jong S, Suurmeijer AJH, Meijer C, van der Graaf WTA. The insulin-like growth factor system and sarcomas. J Pathol 2008;217: 469–82.
23. Mohammadi M, Olsen SK, Ibrahimi OA. Structural basis for fibroblast growth factor receptor activation. Cytokine & Growth Factor Rev 2005;16:107–37.
24. Kamura S, Matsumoto Y, Fukushi J, Fujiwara T, Iida K, Okada Y, et al. Basic fibroblast growth factor in the bone microenvironment enhances cell motility and invasion of Ewing's sarcoma family of tumours by activating the FGFR1-PI3K-Rac1 pathway. Br J Cancer 2010;103: 370–81.
25. Lai JP, Chien J, Strome SE, Staub J, Montoya DP, Greene EL, et al. HSulf-1 modulates HGF-mediated tumor cell invasion and signaling in head and neck squamous carcinoma. Oncogene 2003;23: 1439–47.
26. Karajannis MA, Vincent L, DiRenzo R, Shmelkov SV, Zhang F, Feldman EJ, et al. Activation of FGFR1β signaling pathway promotes survival, migration and resistance to chemotherapy in acute myeloid leukemia cells. Leukemia 2006;20:979–86.

Published OnlineFirst on January 6, 2012; DOI:10.1158/1541-7786.MCR-11-0347

27. Kwabi-Addo B, Ozen M, Ittmann M. The roles of fibroblast growth factors and their receptors in prostate cancer. Endocr Relat Cancer 2004;11:709–24.
28. Montero A, Okada Y, Tomita M, Ito M, Tsurukami H, Nakamura T, et al. Disruption of the fibroblast growth factor-2 gene results in decrease bone mass and bone formation. J Clin Invest 2000;105:1085–93.
29. Marie PJ. Fibroblast growth factor signaling controlling osteoblast differentiation. Gene 2003;316:23–32.
30. Ware CB, Horowitz MC, Renshaw BR, Hunt JS, Liggitt D, Koblar SA, et al. Targeted disruption of the low-affinity leukemia inhibitory factor receptor gene causes placental, skeletal, neural and metabolic defects and results in perinatal death. Development 1995;121:1283–99.
31. Soube T, Naganawa T, Xiao L, Okada Y, Tanaka Y, Ito M, et al. Over-expression of fibroblast growth factor-2 causes defective bone mineralization and osteopenia in transgenic mice. J Cell Biochem 2005;95:83–94.
32. Coffin JD, Florkiewicz RZ, Neumann J, Mort-Hopkins T, Dorn GW, Lightfoot P, et al. Abnormal bone growth and selective translational regulation in basic fibroblast growth factor (FGF-2) transgenic mice. Mol Biol Cell 1995;6:1861–73.
33. Pitaru S, Kotev-Emeth S, Noff D, Kaffuler S, Savion N. Effect of basic fibroblast growth factor on the growth and differentiation of adult stromal bone marrow cells: Enhanced development of mineralized bone-like tissue in culture. J Bone Miner Res 1993;8:19–29.
34. Nagai H, Tsukuda R, Mayahara H. Effects of basic fibroblast growth factor (bFGF) on bone formation in growing rats. Bone 1995;16:367–73.
35. Nakamura T, Harada K, Tamura M, Shibanushi T, Nigi H, Tagawa M, et al. Stimulation of endosteal bone formation by systemic injections of recombinant basic fibroblast growth factor in rats. Endocrinology 1995;136:1276–84.
36. Hurley MM, Abreu C, Harrison JR, Lichtler AC, Raisz LG, Kream BE. Basic fibroblast growth factor inhibits Type I Collagen gene expression in osteoblastic MC-3T3-E1 cells. J Biol Chem 1993;268:5588–93.
37. Debiais F, Hott M, Graulet AM, Marie PJ. The effects of fibroblast growth factor-2 on human neonatal calvaria osteoblastic cells are differentiation stage specific. J Bone Mier Res 1998;13:645–55.
38. Canalis E, Centrella M, McCarthy T. Effects of basic fibroblast growth factor on bone formation *in vitro*. J Clin Invest 1988;81:1572–7.
39. Malaval L, Aubin JE. Biphasic effects of leukemia inhibitory factor on osteoblastic differentiation. J Cell Biochem Suppl 2001;Suppl 36: 63–70.
40. Ge C, Xiao G, Jiang D, Franceschi RT. Critical role of the extracellular signal-regulated kinase-MAPK pathway in osteoblast differentiation and skeletal development. J Cell Biol 2007;176: 709–18.
41. Schindeler A, Little DG. Ras-MAPK signaling in osteogenic differentiation: friend or foe? J Bone Miner Res 2006;21:1331–8.
42. Kawasaki T, Niki Y, Miyamoto T, Horiuchi K, Matsumoto M, Aizawa M, et al. The effect of timing in the administration of hepatocyte growth factor to modulate BMP-2-induced osteoblast differentiation. Biomaterials 2010;31:1191–8.
43. Neto AHC, Queiroz KC, Milani R, Paredes-Gamero EJ, Justo GZ, Peppelenbosch MP, et al. Profiling the changes in signaling pathways in ascorbic acid/β-glycerophosphate-induced osteoblastic differentiation. J Cell Biochem 2011;112:71–7.
44. Bikfalvi A, Klein S, Pintucci G, Rifkin DB. Biological roles of fibroblast growth factor-2. Endocr Rev 1997;18:26–45.
45. Yu PJ, Ferrari G, Galloway AC, Mignatti P, Pintucci G. Basic fibroblast growth factor (FGF-2): The high molecular weight forms come of age. J Cell Biochem 2007;100:1100–8.
46. Sturla LM, Westwood G, Selby PJ, Lewis IJ, Burchill SA. Induction of cell death by basic fibroblast growth factor in Ewing's sarcoma. Cancer Res 2000;60:6160–70.
47. Kim MS, Kim CJ, Jung HS, Seo MR, Juhnn YS, Shin HY, et al. Fibroblast growth factor 2 induces differentiation and apoptosis of Askin tumor cells. J Pathol 2004;202:103–12.
48. Nissen LJ, Cao R, Hedlund EM, Wang Z, Zhao X, Wetterskog D, et al. Angiogenic factors FGF2 and PDGF-BB synergistically promote murine tumor neovascularization and metastasis. J Clin Invest 2007; 117:2766–77.
49. Haugsten EM, Wiedlocha A, Olsnes S, Wescha J. Roles of fibroblast growth factor receptors in carcinogenesis. Mol Cancer Res 2010; 8:1439–52.
50. Manolagas SC. Birth and death of bone cells: basic regulatory mechanisms and implications for the pathogenesis and treatment of osteoporosis. Endocr Rev 2000;21:115–37.

THE JOURNAL OF BIOLOGICAL CHEMISTRY VOL. 287, NO. 2, pp. 1397–1405, January 6, 2012

Competitive Interactions of Cancer Cells and Normal Cells via Secretory MicroRNAs*[S]

Received for publication, August 4, 2011, and in revised form, November 23, 2011 Published, JBC Papers in Press, November 28, 2011, DOI 10.1074/jbc.M111.288662

Nobuyoshi Kosaka[‡1], **Haruhisa Iguchi**[‡§1], **Yusuke Yoshioka**[‡2], **Keitaro Hagiwara**[‡¶], **Fumitaka Takeshita**[‡], **and Takahiro Ochiya**[‡3]

From the [‡]*Division of Molecular and Cellular Medicine, National Cancer Center Research Institute, 5-1-1, Tsukiji, Chuo-ku, Tokyo 104-0045, Japan,* [§]*Pharmacology Research Laboratories, Dainippon Sumitomo Pharma Co., Ltd., 1-98, Kasugadenaka 3-chome, Konohana-ku, Osaka 554-0022, Japan, and the* [¶]*Department of Biological Information, Graduate School of Bioscience and Biotechnology, Tokyo Institute of Technology, Yokohama, Kanagawa 226-8501, Japan*

Background: Homeostatic cell competitive system between cancerous cells and non-cancerous cells is considered as the reason for tumor initiation.
Results: Exosomal tumor-suppressive microRNAs secreted by non-cancerous cells inhibit the proliferation of cancerous cells.
Conclusion: Exosomal tumor-suppressive microRNAs act as an inhibitory signal for cancer cells in a cell-competitive process.
Significance: This provides a novel insight into a tumor initiation mechanism.

Normal epithelial cells regulate the secretion of autocrine and paracrine factors that prevent aberrant growth of neighboring cells, leading to healthy development and normal metabolism. One reason for tumor initiation is considered to be a failure of this homeostatic cell competitive system. Here we identify tumor-suppressive microRNAs (miRNAs) secreted by normal cells as anti-proliferative signal entities. Culture supernatant of normal epithelial prostate PNT-2 cells attenuated proliferation of PC-3M-luc cells, prostate cancer cells. Global analysis of miRNA expression signature revealed that a variety of tumor-suppressive miRNAs are released from PNT-2 cells. Of these miRNAs, secretory miR-143 could induce growth inhibition exclusively in cancer cells *in vitro* and *in vivo*. These results suggest that secretory tumor-suppressive miRNAs can act as a death signal in a cell competitive process. This study provides a novel insight into a tumor initiation mechanism.

Competitive interactions among cells are the basis of many homeostatic processes in biology. In *Drosophila*, normal epithelial cells compete with transformed ones for individual survival, which is a process called cell competition (1, 2). If a given group of cells was exposed to some stress, it would be separated into subpopulations of cells with different levels of damage. In noncompetitive conditions, cells with severe damage die in a short time, whereas moderately damaged cells survive to the next generation, indicative of the transduction of a negative phenotype. On the other hand, in competitive conditions even slightly damaged cells are eliminated from the cell group because healthy cells, the "winners," convey death signals to damaged cells, the "losers," and the losers reciprocally confer growth signals to the winners. This feed-forward regulation enables the cell population to eradicate abnormal cells and maintain the same number of normal cells in a limited niche.

Oncogenesis is characterized by genetic and metabolic changes reprogramming living cells to undergo uncontrolled proliferation (3). This suggests that the abnormal cells that are originally destined for elimination can survive and expand against the cell competitive regulation, leading to the formation of a tumor mass. Consistently with this concept, Bondar and Medzhitov (4) showed that the cell competition process involves p53, a tumor-suppressive gene, between the hematopoietic stem cells and progenitor cells, suggesting that gene modifications of p53 could disturb the homeostatic mechanism and give rise to tumor initiation. It is conceivable that p53 target genes could be associated with intercellular communication between winners and losers; however, this literature has not answered the question of whether this regulatory system is mediated by contact-dependent or contact-independent manner. More than 10 years ago a pioneer study suggested that non-cancerous cells co-cultured with cancer cells inhibit the growth of cancer cells *in vitro* (5). This result indicated that humoral factors could be involved in cell competition as intercellular communicators (6).

As recently as a few years ago it was believed that RNAs could not behave as extracellular signal molecules because of their vulnerability to the attack of ribonucleases largely existing in body fluid. Evidence is presently increasing to show that miRNAs[4] contained in exosomes are released from mammalian

* This work was supported in part by a grant-in-aid for the Third-Term Comprehensive 10-Year Strategy for Cancer Control, a grant-in-aid for Scientific Research on Priority Areas Cancer from the Ministry of Education, Culture, Sports, Science, and Technology, the Program for Promotion of Fundamental Studies in Health Sciences of the National Institute of Biomedical Innovation, and the Japan Society for the Promotion of Science through the "Funding Program for World-Leading Innovative R&D on Science and Technology (FIRST Program)" initiated by the Council for Science and Technology Policy.
[S] This article contains supplemental Figs. 1–3.
[1] Both authors contributed equally to this work.
[2] A Research Fellow of the Japan Society for the Promotion of Science.
[3] To whom correspondence should be addressed: Division of Molecular and Cellular Medicine, National Cancer Center Research Institute, 1-1, Tsukiji, 5-chome, Chuo-ku, Tokyo 104-0045, Japan. Tel.: 81-3-3542-2511 (ext. 4800); Fax: 81-3-3541-2685; E-mail: tochiya@ncc.go.jp.

[4] The abbreviations used are: miRNA, microRNA; CM, conditioned medium; luc, luciferase; MTT, 3-(4,5-dimethylthiazol-2-yl)-2,5-diphenyltetrazolium bromide; QRT-PCR, quantitative real time PCR.

cells and act as a signal transducer (7). It is important that many different tumor-suppressive miRNAs, such as miR-16 and miR-143, are down-regulated in cancer cells, resulting in tumorigenesis, tumor progression, and metastasis (8–11). Taken together, these findings suggest that secretory miRNAs may have favorable aspects for anti-proliferative signals mediating cell competition.

In this report we show that miR-143 expression in normal prostate cells, PNT-2 cells, is higher than that in prostate cancer cells, PC-3M-luc cells, and that miR-143 released from non-cancerous cells transfers growth-inhibitory signals to cancerous cells *in vitro* and *in vivo*. These results suggest that secretory tumor-suppressive miRNAs might be a death signal from winners to losers in the context of cell competition. Secretory miRNAs can be conducive to the maintenance of normal growth and development.

EXPERIMENTAL PROCEDURES

Reagents—Mouse monoclonal anti-KRAS (F234) (sc-30) was purchased from Santa Cruz. Rabbit polyclonal anti-ERK5 (#3372) was purchased from Cell Signaling. Mouse monoclonal anti-actin, clone C4 (MAB1501), was obtained from Millipore. Mouse monoclonal ant-human-CD63 antibody (556019) was purchased from BD Pharmingen. Peroxidase-labeled anti-mouse and anti-rabbit antibodies were included in the Amersham Biosciences ECL PLUS Western blotting Reagents Pack (RPN2124) (GE Healthcare). Synthetic *Caenorhabditis elegans* miRNA cel-miR-39 was synthesized by Qiagen (Valencia, CA). Synthetic hsa-miR-143 (pre-miR-143), the negative control 1 (NC1), has-miR-143 inhibitor molecule (anti-miR-143), and the negative control inhibitor molecule (anti-NC) were purchased from Ambion (Austin, TX). GW4869 was purchased from Calbiochem. Geneticin was purchased from Invitrogen.

Cell Culture—PNT-2 cells, immortalized normal adult prostatic epithelial cell line, were purchased from the DS Pharma Biomedical Co., Ltd. (Osaka, Japan). HEK293 cells, a human embryonic kidney cell line (CRL-1573), were obtained from American Type Culture Collection (Manassas, VA). HEK293 cells were cultured in Dulbecco's modified Eagle's medium containing 10% heat-inactivated fetal bovine serum (FBS) and an antibiotic-antimycotic (Invitrogen) at 37 °C in 5% CO_2. PNT-2 and the prostate cancer cell line, PC-3M-luc cells, continuously expressing firefly luciferase (Xenogen, Alameda, CA), were cultured in RPMI containing 10% heat-inactivated FBS and an antibiotic-antimycotic at 37 °C in 5% CO_2.

Preparation of Conditioned Medium and Exosomes—Before the collection of culture medium, cells were washed 3 times with Advanced RPMI containing an antibiotic-antimycotic and 2 mM L-glutamine (medium A), and the medium was switched to fresh medium A. After incubation for 3 days, medium A was collected and centrifuged at 2000 × *g* for 10 min at room temperature. To thoroughly remove cellular debris, the supernatant was centrifuged again at 12,000 × *g* for 30 min at room temperature or filtered through a 0.22-μm filter (Millipore). The conditioned medium (CM) was then used for miRNA extraction and functional assays as well as exosome isolation.

For exosome preparation the CM was ultracentrifuged at 110,000 × *g* for 70 min at 4 °C. The pellets were washed with 11 ml of PBS, and after ultracentrifugation they were resuspended in PBS. The exosome fraction was measured for its protein content using the Micro BCA Protein Assay kit (Thermo Scientific, Wilmington, DE).

Isolation of MicroRNAs—Isolation of extracellular and cellular miRNAs was performed using the miRNeasy Mini Kit (Qiagen). Two hundred microliters of conditioned medium or cell lysate was diluted with 1 ml of Qiazol Solution. After 5 min of incubation, 10 μl of 0.1 nM cel-miR-39 was added to each aliquot followed by vortexing for 30 s. Subsequent extraction and filter cartridge work were carried out according to the manufacturer's protocol.

Quantitative Real Time PCR (QRT-PCR)—The method for QRT-PCR has been previously described (7). PCR was carried out in 96-well plates using the 7300 Real Time PCR System (Applied Biosystems). All reactions were done in triplicate. All TaqMan MicroRNA Assays were purchased from Applied Biosystems. Cel-miR-39 and RNU6 were used as an invariant control for the CM and cells, respectively.

Immunoblot Analysis—SDS-PAGE gels, SuperSep Ace 5–20% (194–15021) (Wako), were calibrated with Precision Plus Protein Standards (161–0375) (Bio-Rad), and anti-KRAS (1:100), anti-ERK5 (1:1000), anti-CD63 (1:200), and anti-actin (1:1000) were used as primary antibodies. The dilution ratio of each antibody is indicated in parentheses. Two secondary antibodies (peroxidase-labeled anti-mouse and anti-rabbit antibodies) were used at a dilution of 1:10,000. Bound antibodies were visualized by chemiluminescence using the ECL PLUS Western blotting detection System (RPN2132) (GE Healthcare), and luminescent images were analyzed by a LuminoImager (LAS-3000; Fuji Film, Inc.). Only gels for CD63 (BD Biosciences) detection were run under non-reducing conditions.

Plasmids—The primary-miR-143 expression vector was purchased from TaKaRa BIO. For luciferase-based reporter gene assays, pLucNeo was constructed by inserting a firefly luciferase gene derived from the pGL3-control (Promega) into the pEYFP-1 vector (Clontech) at BglII and AflII sites. The sensor vector for miR-143 was constructed by introducing tandem binding sites with perfect complementarity to miR-143 separated by a four-nucleotide spacer into the NotI site of psiCHECK2 (Promega). The sequences of the binding site are as follows: 5′-AAACCTAGAGCGGCCGCGAGCTACAGTGCT***TCATCTC***AAAGAATTCTTGAGCTACAGTGCT***TCATCTC***AGCGGCCGCTGGCCGCAA-3′ (sense) and 5′-TTGCGGCCAGCGGCCGCTGAGATGAAGCACTGTAGCTCAAGAATTCTTTGAGATGAAGCACTGTAGCTCGCGGCCGCTCTAGGTTT-3′ (antisense). The "seed" sequence of miR-143 is indicated by bold italics. In a mutated miR-143 sensor vector, the seed sequence, TCATCTC, was displaced with GACGAGA. All the plasmids were verified by DNA sequencing.

Transient Transfection Assays—Transfections of 10 nM miR-143 mimic and 3 nM anti-miR-143 were accomplished with the DharmaFECT Transfection Reagent (Thermo Scientific) according to the manufacturer's protocol. The total amounts of miRNAs for each transfection were equally adjusted by the addition of NC1 and anti-NC, respectively.

Establishment of Stable Cell Lines—Stable HEK293 cell lines that express miR-143 were generated by selection with 300 μg/ml Geneticin. HEK293 cells were transfected with 0.5 μg of the pri-miR-143 expression vector at 90% confluency in 24-well dishes using a Lipofectamine LTX reagent in accordance with the manufacturer's instructions. Twelve hours after the transfection, the cells were re-plated in a 10-cm dish followed by a 3-week selection with the antibiotic. Ten surviving single colonies were picked up from each transfectant and then cultured for another 2 weeks. The cells expressing the largest amount of miR-143 among transfectants were used as miR-143 stably expressing cells.

Luciferase Reporter Assay—HEK293 cells were cultured at a density of 1×10^4 cells/well in 96-well tissue culture plates overnight, and miRNA transfections or the addition of CM was performed. The cells were harvested, and renilla luciferase activity was measured and normalized by firefly luciferase activity (10). All assays were performed in triplicate and repeated at least three times, and the most representative results are shown.

Cell Growth Assay—PC-3M-luc cells were seeded at a density of 2×10^3 cells/well in a 96-well plate. The following day the cells were transfected with mature miRNAs or incubated with a CM. Twenty-four hours later the culture medium of the transfected cells was switched to medium A, whereas the conditioned medium was not changed. After a 3-day culture, cells were harvested for the measurement of firefly luciferase activity. To know the cellular proliferation by the tetrazolium-based colorimetric MTT assay, 20 μl CM of TetraColor ONE (SEIKAGAKU Corp., Tokyo, Japan) was added to each well after 72 h of culture. After 2–4 h of incubation at 37 °C, the optical density was measured at a wavelength of 450 nm using a microplate reader.

PKH67-labeled Exosome Transfer—Purified exosomes derived from PNT-2 CM were labeled with a PKH67 green fluorescent labeling kit (Sigma). Exosomes were incubated with 2 μM PKH67 for 5 min, washed 4 times using a 100-kDa filter (Microcon YM-100, Millipore) to remove excess dye, and incubated with PC-3M-luc cells at 37 °C.

Co-culture Experiment—In co-culture experiments, 2×10^5 cells/well of PNT-2 cells were plated in 6-well plates. To stain the PNT-2 cells with BODIPY-TR-ceramide (Invitrogen), 5 μM BODIPY-TR-ceramide in a non-serum culture medium was added and incubated with the cells at 37 °C. After 30 min the cells were rinsed several times with a non-serum culture medium and incubated in a fresh medium at 37 °C for an additional 30 min. After the staining of PNT-2 cells by BODIPY-TR-ceramide, labeling of PC-3M-luc cells with PKH67 was performed in accordance with the manufacturer's instructions. After that, labeled PC-3M-luc cells were added and co-cultured with PNT-2 cells for 12 h at 37 °C.

Microarray Analysis—To detect the miRNAs in exosomes and cells derived from PNT-2 and PC-3M-luc cells, 100 ng of total RNA was labeled and hybridized using a human microRNA microarray kit (Agilent Technologies) according to the manufacturer's protocol (Protocol for Use with Agilent MicroRNA Microarrays Version 1.5). Hybridization signals were detected using a DNA microarray scanner (Agilent Technologies), and the scanned images were analyzed using Agilent Feature Extraction software.

Evaluation of Tumor-suppressive miRNA Delivery to Subcutaneously Implanted Prostate Cancer Cell Line in Mice—Animal experiments in this study were performed in compliance with the guidelines of the Institute for Laboratory Animal Research, National Cancer Center Research Institute. Seven-week-old male Balb/c athymic nude mice (CLEA Japan, Shizuoka, Japan) were anesthetized by exposure to 3% isoflurane for injections and *in vivo* imaging. Four days ahead of the first CM injection, the anesthetized animals were subcutaneously injected with 5×10^5 PC-3M-luc cells suspended in 100 μl of sterile Dulbecco's phosphate-buffered saline into each dorsal region. Five hundred μl of CM derived from miR-143-overexpressing HEK293 cells and control cells were daily injected into each tumor from day 0 to 6. For *in vivo* imaging, the mice were administered D-luciferin (150 mg/kg, Promega) by intraperitoneal injection. Ten minutes later, photons from animal whole bodies were counted using the IVIS imaging system (Xenogen) according to the manufacturer's instructions. Data were analyzed using LIVINGIMAGE 2.50 software (Xenogen).

RESULTS

Suppression of Prostate Cancer Cell Proliferation by Conditioned Medium Isolated from Non-cancerous Prostatic Cell—Cell competition is a homeostatic mechanism for the accommodation of an appropriate number of cells in a limited niche or stroma (1). Based on this idea it is possible that the cell competition between normal and abnormal cells frequently occurs in a precancerous state. Of note is that non-cancerous cells suppress cancer cell development by contact-independent interaction (12). For instance, endothelial cells provide the major extracellular heparan sulfate proteoglycan as anti-proliferative signals (12); however, the molecular mechanism by which the other types of cells in a tumor environment associate with cancer cells is not fully understood.

To analyze the mechanism, we treated a hormone-insensitive prostatic carcinoma cell line, PC-3M-luc cells, with a CM from the non-cancerous prostate cell line PNT-2 cells. After a 3-day incubation, the PNT-2 CM inhibited the growth of the PC-3M-luc cells up to ~10% compared with the cell growth treated by fresh culture medium (Fig. 1*A*; compare *lanes 1* and *3*). In contrast, the growth of PC-3M-luc cells incubated in the CM of PC-3M-luc cells themselves showed no inhibitory effect (Fig. 1*A*; compare *lanes 1* and *2*). To determine that the performed treatments did not affect the luciferase activity, we also used the colorimetric MTT assay to measure the cell growth of PC-3M-luc cells. As shown in supplemental Fig. 1*A*, not only luciferase assay but also MTT assay show the inhibition of PC-3M-luc cell proliferation by the addition of PNT-2 cells derived CM, indicating that our treatment did not affect the luciferase activity. These results indicate that the non-cancerous cells may secrete some molecules that can suppress cancer cell proliferation.

In a recent report we showed that miRNAs contained in exosomes are secreted and that their secretion is tightly regulated by neutral sphingomyelinase 2, which is known to hydrolyze sphingomyelins to generate ceramides and trigger the budding

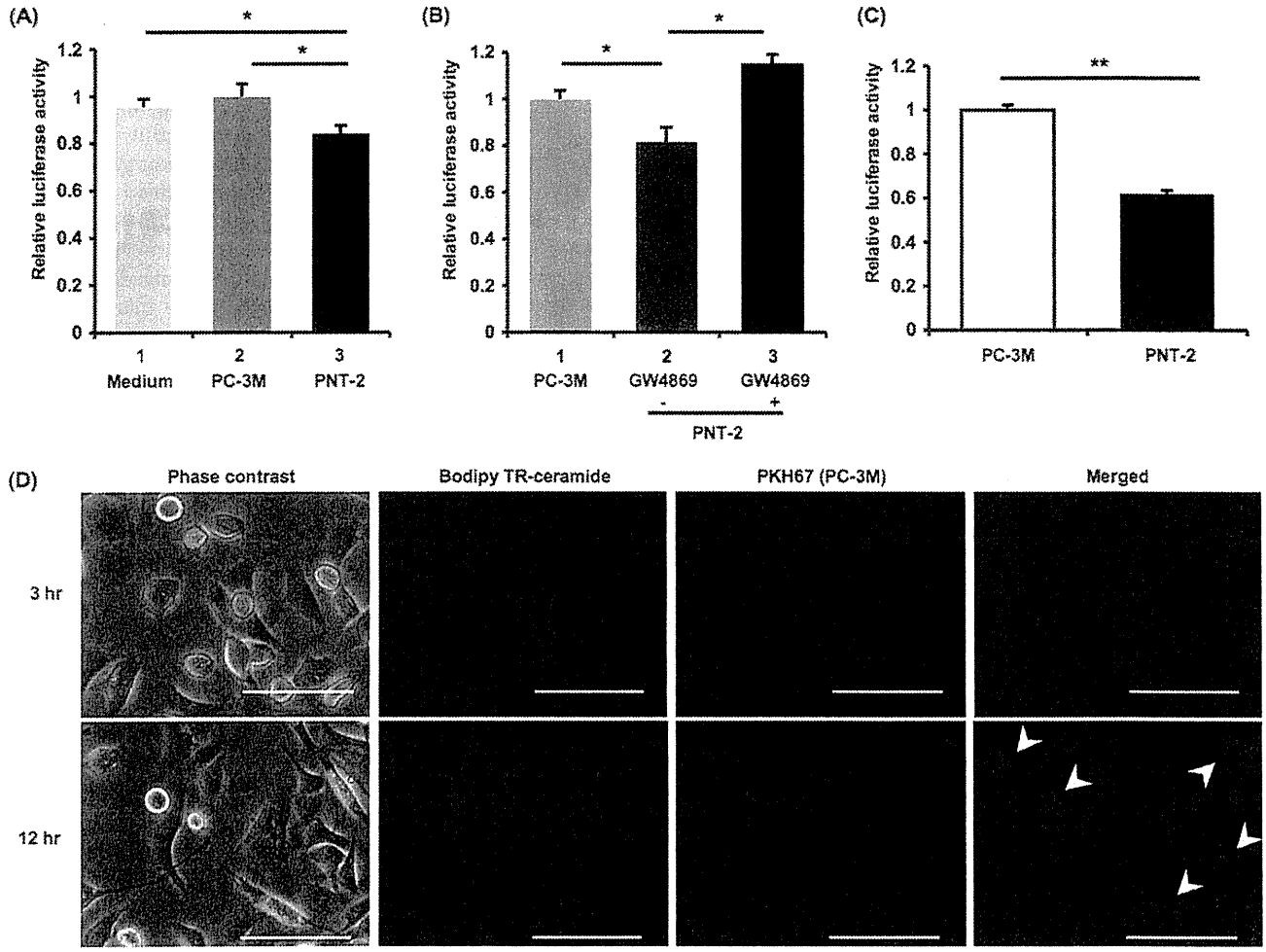

FIGURE 1. **Suppression of cancerous cell proliferation by exosome isolated from non-cancerous cells.** *A*, cell growth inhibition by a conditioned medium derived from PNT-2 cells is shown. PC-3M-luc cells were incubated for 3 days in a conditioned medium isolated from PC-3M-luc cells, PNT-2 cells, or a culture medium followed by a cell growth assay as described under "Experimental Procedures." The values on the *y* axis are depicted relative to the normalized luciferase activity of culture medium-treated cells, which is defined as 1. Each *bar* is presented as the mean S.E. ($n = 3$). *, $p < 0.05$ as compared with culture medium-treated PC-3M-luc cells; Student's *t* test. *B*, treatment with GW4869 to donor cells restored the reduced cell growth by the PNT-2-derived CM is shown. Donor PNT-2 cells were incubated in the presence or absence of 10 μM GW4869 for 2 days. The conditioned medium from PC-3M-luc cells was used as a control. The values on the *y* axis are depicted relative to the normalized luciferase activity of PC-3M-luc-conditioned medium-treated cells, which is defined as 1. Each *bar* is presented as the mean S.E. ($n = 3$). *, $p < 0.05$; Student's *t* test. *C*, cell growth inhibition by exosomes derived from PNT-2 cells is shown. PC-3M-luc cells were incubated in exosomes isolated from PNT-2 cells or PC-3M-luc cells followed by a cell growth assay, as described under "Experimental Procedures." The values on the *y* axis are depicted relative to the normalized luciferase activity of cells treated with exosomes derived from PC-3M-luc cells is defined as 1. Each *bar* is presented as the mean S.E. ($n = 3$). **, $p < 0.005$, as compared with exosomes isolated from PC-3M-luc cells; Student's *t* test. *D*, shown are fluorescent photos of BODIPY-ceramide-labeled PNT-2 and PC-3M-luc cells marked by PKH67. PNT-2 cells and PC-3M-luc cells were labeled with red fluorescent BODIPY-ceramide and green fluorescent PKH67, respectively, as described under "Experimental Procedures." After treatment of PNT-2 by BODIPY-ceramide, PKH67-labeled PC-3M-luc cells were added. After co-culturing for 3 or 12 h, images were obtained. Fluorescent photos were detected with the Eclipse TE 2000 Inverted Research Microscope, and images were produced using NIS-Elements BR software. *Arrowheads* show *yellow colored* cancer cells. The *size bar* indicates 100 μm.

of exosomes. We collected two separate aliquots of CM from PNT-2 cells incubated with or without GW4869, a specific inhibitor for neutral sphingomyelinase 2. The isolated exosomes were verified by the detection of CD63 protein, a well established exosome marker, with immunoblotting (supplemental Fig. 1*B*), and the activity of GW4869 was confirmed by the decreased amount of exosomal protein (supplemental Fig. 1*C*). The CM prepared in the presence of the GW4869 compound cancelled most tumor-suppressive activity of the non-treated PNT-2 CM (Fig. 1*B*; compare *lanes 1–3*). Furthermore, proliferation of PC-3M-luc cells was inhibited by the addition of the exosome fraction isolated from the PNT-2 CM by ultracentrifugation (Fig. 1*C*). These observations suggest that exosomal miRNAs derived from non-cancerous cells were transferred to cancerous cells, resulting in the inhibition of their proliferation.

To visualize the transfer of ceramide-containing exosome from PNT-2 to PC-3M-luc *in vitro*, a co-culture experiment was performed. Before the co-culture, 2×10^5 PNT-2 cells were incubated for 30 min with red fluorescent BODIPY-ceramide dye, which can label the exosomes inside the cells (13, 14). After washing five times with PBS, equal numbers of PC-3M-luc cells labeled by green fluorescent PKH67, a cellular membrane indicator, were added into the culture dishes. Three hours later we did not observe any PC-3M-luc cells with a yellow color (*Merged* photo in *upper panel* of Fig. 1*D*), indicating that car-

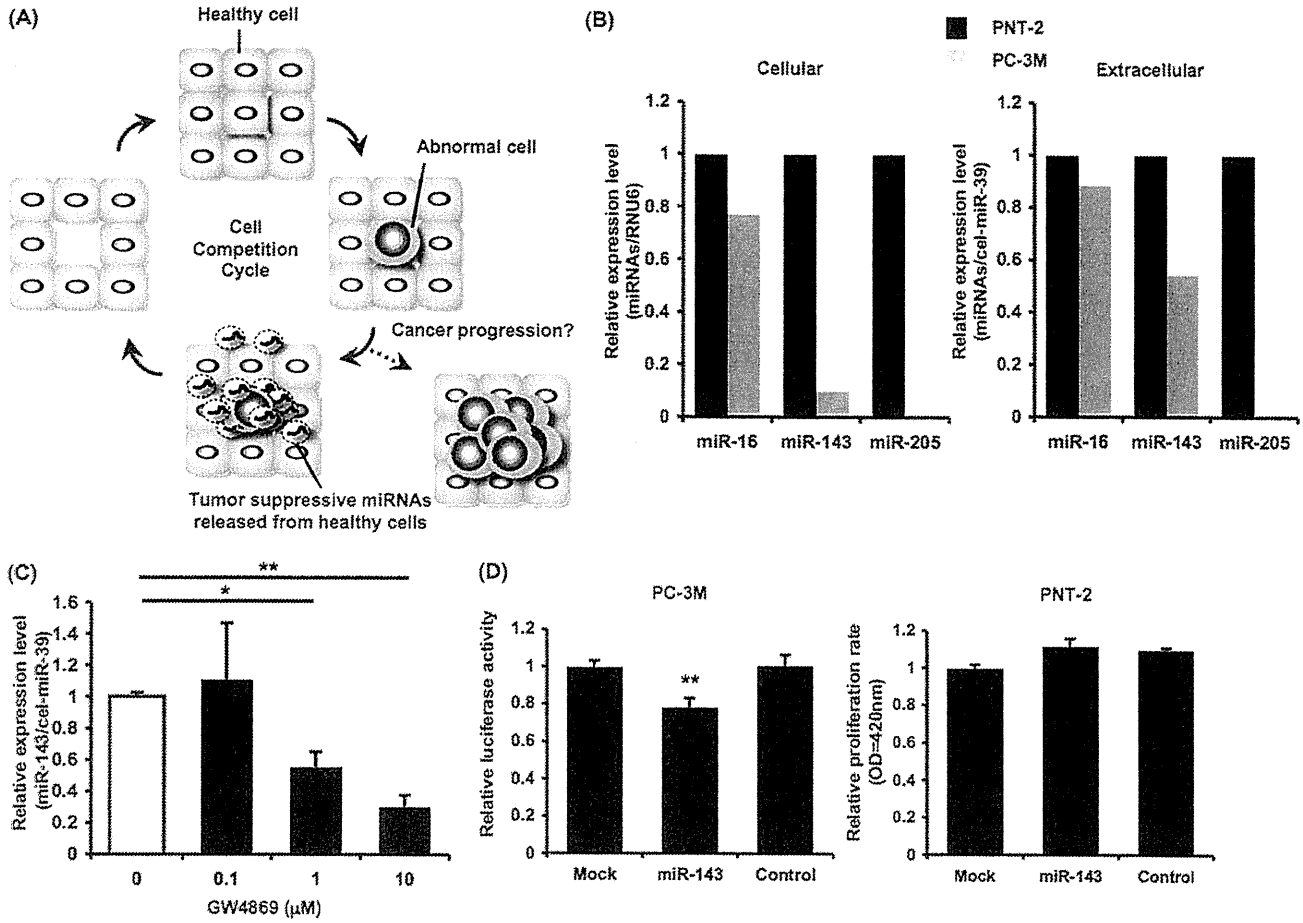

FIGURE 2. **Down-regulation of cellular and extracellular tumor-suppressive miRNAs in PC-3M-luc cells.** *A*, shown is a schematic representation of hypothetical tumor initiation process. Neighboring healthy cells (*blue*) secrete tumor-suppressive miRNAs (*light yellow*) to inhibit the proliferation of abnormal cells (gray), and this cell population returns to the initial healthy condition (a homeostatic cycle). Once the cell competitive cycle is compromised, this niche become susceptible to tumor initiation (indicated by a *dashed arrow*). *B*, comparison of cellular and extracellular miRNAs expression in PNT-2 and PC-3M-luc cells is shown. miRNA expression levels were determined by a Taq-Man QRT-PCR. The values on the *y* axis are depicted relative to the normalized expression level of PNT-2 cells, which is defined as 1. *C*, secretion of miR-143 was suppressed by the treatment with GW4869. PNT-2 cells were seeded and cultured in a 24-well plate for 48 h in the indicated concentrations of GW4869. After the incubation, the medium was subjected to QRT-PCR for miR-143. The values on the *y* axis are depicted relative to the amount of miR-143 at 0 μM GW4869, which is defined as 1. *D*, shown is cell growth inhibition by miR-143 in PC-3M-luc cells but not in PNT-2 cells. PNT-2 and PC-3M-luc cells were transfected with 10 nM miR-143 molecules (miR-143) or 10 nM negative control molecules (control) or without RNA molecules (*Mock*). The values on the *y* axis are depicted relative to the normalized luciferase activity of untreated cells (*Mock*), which is defined as 1. Each *bar* is presented as the mean S.E. ($n = 3$). *, $p < 0.05$; **, $p < 0.005$, as compared with untreated PC-3M-luc cells; Student's *t* test.

ried-over red dyes were thoroughly removed as 3 h is enough time for the dye to be incorporated directly into the cells. By contrast, after 12 h of co-culture, yellow fluorescence was observed in green-labeled PC-3M-luc cells (indicated by *arrowheads* in Merged photo in the *lower panel* of Fig. 1*D*), suggesting that ceramide-containing exosomes from PNT-2 cells were transferred to the PC-3M-luc cells. This result is corroborated by the uptake experiment using the PKH67-labeled exosomes purified from PNT-2 culture medium (supplemental Fig. 1*D*). Green fluorescence was detected in PC-3M-luc cells after 16 h of incubation, providing a direct evidence for exosome uptake by cancerous cells.

Tumor-suppressive miRNAs Down-regulated in Cancerous Cells Were Secreted from Non-cancerous Cells—We propose a hypothetical model of tumor initiation involving cell competition and anti-proliferative secretory miRNAs (Fig. 2*A*). In a cell competition cycle, as illustrated in the *bottom part* of Fig. 2*A*, growth inhibitory miRNAs are actively released from non-cancerous cells to kill abnormal cells with a partial oncogenic ability, thereby restoring them to a healthy state. Indeed, inhibitory capacity of these miRNAs appears to be limited in the setting of single treatment with the PNT-2 CM (Fig. 1*A*); however, they can potentially prevent emergence of tumor cells in a physiological condition. Because abundantly existing healthy cells continuously provide nascent overproliferative cells with tumor-suppressive miRNAs for a long period, a local concentration of secretory miRNAs can become high enough to restrain a tumor initiation. A *dashed arrow* in Fig. 2*A* indicates the way whereby the disruption of the homeostatic system leads to tumor expansion. If precancerous cells acquire resistance to anti-proliferative secretory miRNAs or normal cells cannot supply an adequate amount of miRNAs, then this defensive system will fail to maintain the healthy condition.

To test this hypothesis we checked the secretion amount of representative tumor-suppressive miRNAs by comparing PNT-2 and PC-3M-luc cells with Taq-Man QRT-PCR analysis. As shown in Fig. 2*B*, miR-16, miR-205, and miR-143, which are already reported to be dysregulated in prostate cancer (10, 15, 16), were down-regulated in PC-3M-luc cells at a cellular and extracellular level. The GW4869 inhibitor suppressed the secretion of miR-143 from PNT-2 cells in a dose-dependent manner (Fig. 2*C*), whereas its cellular level was not altered (supplemental Fig. 2*A*). Additionally, the application of small interfering RNAs specific for human neutral sphingomyelinase 2 gene knocked down its mRNAs, resulting in profound decrease in miR-143 secretion (supplemental Fig. 2, *B* and *C*). On the contrary, the expression of miR-143 in the cells was not changed after the transfection of neutral sphingomyelinase 2 siRNA (supplemental Fig. 2*D*). Taken with the result of Fig. 1*B*, these results suggest that the secreted tumor-suppressive miRNAs are implicated in the process of growth inhibition by PNT-2 CM.

For a global understanding of the expression change of non-cancerous and cancerous cells, we performed an miRNA microarray analysis against cellular and exosomal RNAs purified from PNT-2 and PC-3M-luc cells. In the sub-dataset of secretory exosomal miRNAs from PNT-2 cells, we found 40 miRNAs whose cellular amounts were lowered by one-half in PC-3M-luc cells (Table 1). The selected miRNAs expectedly include several types of tumor-suppressive miRNAs, such as miR-15a, miR-200 family, miR-148a, miR-193b, miR-126, and miR-205 (10, 15, 17–20). This observation supports the idea that secretory tumor-suppressive miRNAs are transferred from non-cancerous cells to cancerous cells, in accordance with the concentration gradient of the miRNA.

We have so far demonstrated that normal cells have a higher secretion of tumor-suppressive miRNAs than cancerous cells; however, it remains unclear whether or not these secreted miRNAs affect the proliferation of cells of their origin. To answer this question, we introduced synthesized miR-143 to both PNT-2 and PC-3M-luc cells and assessed their proliferation rates. After 3 days of transfections, the miR-143 analog induced growth inhibition of PC-3M-luc cells compared with mock and control small RNA transfection (Fig. 2*D*, *left panel*). In contrast, the exogenously transduced miR-143 did not show its anti-proliferative effect in PNT-2 cells (Fig. 2*D*, *right panel*), indicating that excessive miR-143 did not confer an additional growth inhibitory effect on normal cells in which expression of miR-143 is maintained to a physiological level. This finding suggests that animal cells may have their own threshold amount for miRNA activity. The different sensitivity found in different cell types can help secretory miRNAs fulfill their purpose to combat exclusively precancerous cells. It is possible that secretory miRNAs, at least, derived from non-cancerous cells such as PNT-2 cells could supplement growth-suppressive signals that are decreased in cancerous cells. Thus, secreted miR-143 might be involved in the cell competitive regulatory system.

TABLE 1
A list of PNT-2-derived secretory miRNAs that were down-regulated less than 0.5-fold in PC-3M cells compared with PNT-2 cells

miRNAs	Fold change[a]
hsa-miR-141	0.0
hsa-miR-200c	0.0
hsa-miR-886–3p	0.0
hsa-miR-30a*	0.0
hsa-miR-155	0.0
hsa-miR-205	0.0
hsa-miR-224	0.0
hsa-miR-148a	0.0
hsa-miR-130a	0.0
hsa-miR-30a	0.1
hsa-miR-663	0.1
hsa-miR-181a-2*	0.1
hsa-miR-484	0.1
hsa-miR-10a	0.1
hsa-miR-192	0.1
hsa-miR-193b	0.1
hsa-miR-200a	0.1
hsa-miR-429	0.1
hsa-miR-769–5p	0.1
hsa-miR-200b	0.2
hsa-miR-195	0.2
hsa-miR-203	0.2
hsa-miR-7	0.2
hsa-miR-200a*	0.2
hsa-miR-200b*	0.2
hsa-miR-30c	0.2
hsa-miR-126	0.3
hsa-miR-149	0.3
hsa-miR-30d	0.3
hsa-miR-181a	0.3
hsa-miR-30e*	0.3
hsa-miR-365	0.4
hsa-miR-135b	0.4
hsa-miR-454*	0.4
hsa-miR-129*	0.4
hsa-miR-30b	0.4
hsa-miR-181b	0.4
hsa-miR-210	0.4
hsa-miR-455–3p	0.5
hsa-miR-15a	0.5

[a] Fold change of the expression of miRNAs in PC-3M cells compared with PNT-2 cells is indicated.

Secretory miR-143 Inhibited Prostate Cancer Cell Proliferation in Vitro—To examine whether miR-143 released from normal cells exert an anti-proliferative activity, we generated HEK293 cells overexpressing miR-143 by nearly 200-fold compared with control (supplemental Fig. 3*A*). After a 3-day incubation with the CM derived from the miR-143-overproducing HEK293 cells and control HEK293 cells, PC-3M-luc cells showed an ~50% decrease in proliferation (Fig. 3*A*, *lanes 1* and *3*). Importantly, the decrease was recovered by the transfection of anti-miR-143 in PC-3M-luc cells (Fig. 3*A*, *lane 3* and *4*). These data indicate that the growth inhibition is attributable to secretory miR-143 contained in the supernatant of miR-143-overexpressing HEK293 cells. In agreement with the exosome-dependent machinery of miRNA secretion, we observed a similar result by using exosome fractions purified from miR-143-transduced HEK293 cells (Fig. 3*B*).

To further study miRNA transfer on a molecular level, we performed a target gene expression analysis and an miRNA-responsive reporter assay. The immunoblotting analysis shows that the addition of the CM isolated from miR-143-overexpressing HEK293 cells significantly knocked down expression of KRAS, a target gene for miR-143 (21), in PC-3M-luc cells (Fig. 3*C*). In addition, we implemented luciferase analyses using

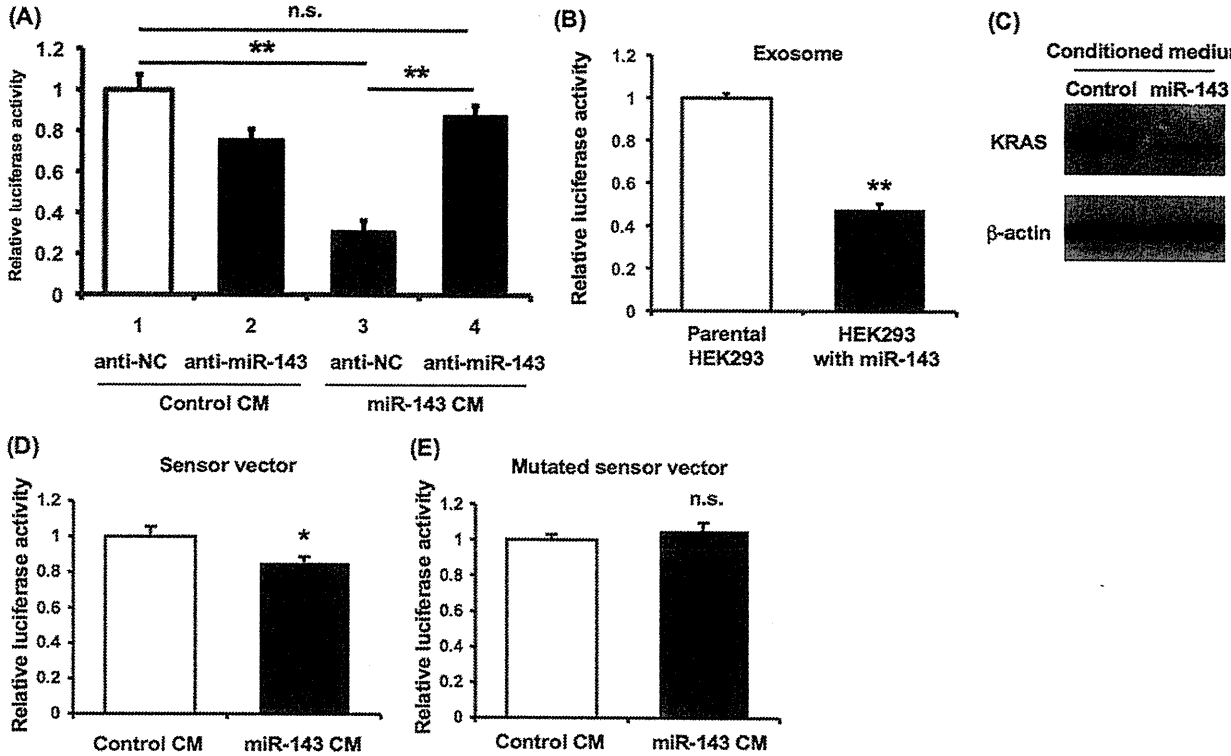

FIGURE 3. **Transfer of secretory miR-143 to PC-3M-luc cells *in vitro*.** *A*, the transfection of anti-miR-143 to PC-3M-luc cells restored the reduced cell growth by the CM derived from miR-143 overproducing cells. After the transfection with 3 nM miR-143 inhibitor molecule (anti-miR-143) (*lanes 2* and *4*) or its control molecule (*anti-NC*) (*lanes 1* and *3*), PC-3M-luc cells were incubated for 3 days in a control conditioned medium (*lanes 1* and *2*) and CM containing extracellular miR-143 (*lane 3* and *4*) followed by a cell growth assay as described under "Experimental Procedures." The values on the *y* axis are depicted relative to the normalized luciferase activity of cells treated in a culture medium, which is defined as 1. Each *bar* is presented as the mean S.E. ($n = 3$). (*, $p < 0.05$; Student's *t* test; *n.s.*, not significant). *B*, cell growth inhibition by exosomes derived from miR-143-transduced HEK293 cells is shown. PC-3M-luc cells were incubated in the exosomes followed by cell growth assay as described under "Experimental Procedures." The values on the *y* axis are depicted relative to the normalized luciferase activity of cells treated with exosomes derived from original HEK293 cells, defined as 1. Each *bar* is presented as the mean S.E. ($n = 3$). (**, $p < 0.005$; Student's *t* test). *C*, secretory miR-143-mediated KRAS suppression in PC-3M-luc cells is shown. Ten micrograms of protein of whole cell lysates prepared from PC-3M-luc cells treated with or without secretory miR-143 were applied to electrophoresis. Immunoblotting was performed with KRAS and actin antibodies and visualized by LAS-3000 system. *D*, extracellular miR-143 derived from HEK293 cells suppressed the luciferase activity of the sensor vector. HEK293 cells transfected with an miR-143 sensor vector were used as recipient cells. The recipient cells were incubated in a CM containing extracellular miRNAs. After a 2-day incubation, a luciferase reporter assay was performed as described under "Experimental Procedures." The values on the *y* axis are depicted relative to the normalized luciferase activity of original HEK293-conditioned medium-treated cells, which is defined as 1. Each *bar* is presented as the mean S.E. ($n = 3$). *, $p < 0.05$; Student's *t* test). *E*, extracellular miR-143 did not reduce the luciferase activity of the mutated sensor vector. HEK293 cells transfected with the mutated miR-143 sensor vector were used as recipient cells. The recipient cells were incubated in a conditioned medium containing extracellular miRNAs. The luciferase assay was carried out as described above. The values on the *y* axis are depicted relative to the normalized renilla luciferase activity of control cells, which is defined as 1. Each *bar* is presented as the mean S.E. ($n = 3$). *n.s.* represents not significant.

a sensor vector harboring renilla luciferase fused in tandem with miR-143 seed sequence in the 3′-UTR. As shown in Fig. 3*D*, the normalized renilla luciferase activities were reduced by the treatment of miR-143-enriched CM derived from HEK293 cells stably expressing miR-143. In contrast, we did not detect any changes of luminescence by using a mutated vector instead of the intact sensor vector (Fig. 3*E*). Furthermore, we quantified cellular amounts of miR-143 in PC-3M-luc cells incubated with CM derived from HEK293 cells or miR-143 overproducing HEK293 cells by QRT-PCR. As shown in supplemental Fig. 3*B*, miR-143 was clearly increased at a cellular level by the treatment of the miR-143 enriched CM. These results indicate that secretory miR-143 exhibits its on-target growth-inhibitory effect in neighboring precancerous cells, thereby suppressing their disordered growth.

Secretory miR-143 Functions as Tumor Suppressor in Vivo—To our knowledge it has never been demonstrated that extracellular tumor-suppressive miRNAs can be transferred into living cells and induce phenotypic change *in vivo*. To address this possibility, we injected CM derived from miR-143 overproducing HEK293 cells or parental HEK293 cells into nude mice implanted with PC-3M-luc cells. Four days after the subcutaneous implantation, we carried out *in vivo* imaging and CM injections according to the timetable shown in Fig. 4*A*. Tumor expansions have been restrained for 8 days with intratumor administrations of miR-143 enriched CM, and consequently the tumor masses shrank by ~0.5-fold on day 8 (Fig. 4*B*). The representative luminescent images of inoculated PC-3M-luc cells on day 8 were shown in Fig. 4*C*. Consistent with the finding that miR-143 did not impair growth activity of non-cancer cells *in vitro* (Fig. 2*D*), no toxicity was observed in these mice (data not shown). In addition, the expressions of miR-143 target genes, such as KRAS and ERK5 (16, 21), were decreased after miR-143-transduced CM injections, indicative of intercellular miRNA transfer *in vivo* (Fig. 4*D*). Thus, our prostate cancer xenograft model suggests that the tumor-suppressive miRNAs

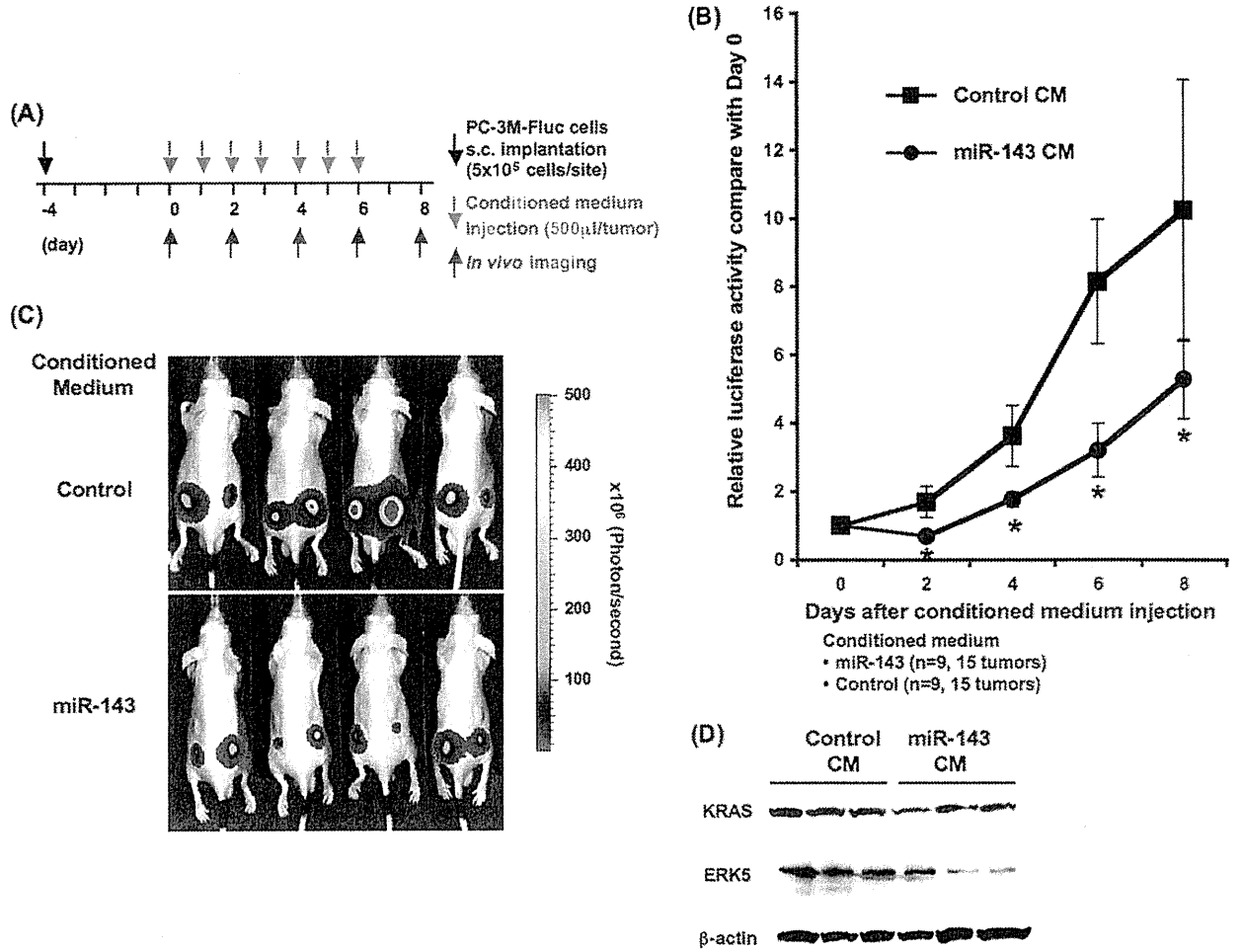

FIGURE 4. **Transfer of secretory miR-143 to PC-3M-luc cells *in vivo*.** *A*, shown is the timetable for conditioned medium injections and *in vivo* imaging. *B*, shown are tumor growth ratios of the inoculated PC-3M-luc cells during the secretory miR-143 treatment. *Closed circles* and *closed squares* indicate the tumor mass administrated with CM from miR-143-overproducing HEK293 cells or parental HEK293 cells, respectively. The values on the *y* axis are depicted relative to the luciferase activity of each tumor on day 0, which is defined as 1. Each *bar* is presented as the mean S.E. ($n = 9$). *, $p < 0.05$; Student's *t* test. *C*, representative images are shown of tumor cells in the skin of mice. Bioluminescence of firefly luciferase from miR-143-enriched CM treated mice and control mice were detected on day 8 with IVIS imaging system. *D*, shown is secretory miR-143-mediated KRAS and ERK5 suppression in inoculated tumor cells. On day 8 the inoculated tumor masses were isolated and applied to immunoblotting analysis for the quantification of KRAS and ERK5 on a protein level.

secreted from normal cells could be efficiently delivered into their neighboring tumors *in vivo*.

DISCUSSION

In this study we documented that miR-143 derived from non-cancerous cells had the ability to suppress the growth of cancer cell proliferation not only *in vitro* but also *in vivo*. These observations suggest that tumor-suppressive miRNAs can be implicated in cell competition between cancer cells and non-cancer cells. In this context, normal cells attempt to prevent the outgrowth of precancerous cells by secreting anti-proliferative miRNAs and maintain a healthy condition; however, the abnormal cells can circumvent this inhibitory machinery, finally resulting in a tumor expansion (Fig. 2*A*). Cell competition could be a homeostatic mechanism that tumor cells need to overcome (1).

Here, we discuss two possible mechanisms by which cancer cells can gain resistance to secretory tumor-suppressive miRNAs. One is a blockade for the uptake of miRNAs, and the other is a cancellation of silencing activity of the incorporated miRNAs. As previously reported, miRNAs are loaded into exosomes and then secreted from living cells (7, 22, 23). If exosomes enriched in miRNAs are actively incorporated by recipient cells, cancer cells can impair the uptake mechanism to escape from the attack of secretory tumor-suppressive miRNAs. This scenario is supported by a recent publication regarding a Tim4 expected for an exosome receptor (24).

In the latter case cancer cells need to specifically compromise the incorporated tumor-suppressive miRNAs because there are some types of miRNAs that are indispensable for the expansion of cancer cells. A RISC assembly is composed of many protein families, such as the mammalian AGO family, GW182, and heat shock proteins (25). Moreover, each gene family also consists of many members, thereby generating diversity of RISC assemblies. The heterogeneity of RISC assemblies allows tumor-suppressive miRNAs to selectively bind with a RISC and silence their target genes on the complex. If cancer cells can exclusively destroy the tumor-suppressive RISC assembly, they can safely

grow in a limited niche full of anti-proliferative miRNAs. The detailed mechanism of the resistance to cell competition remains unknown.

In addition to the acquired resistance, there is another possibility that normal cells will lose secretory capacity of exosomal miRNAs. p53 was shown to enhance exosome production in cells undergoing a p53 response to stress (26). In other words, dysfunction of p53 will result in decreased miRNA secretion. The tumor-suppressive ability of p53 can partly depend on the control of miRNA release from normal cells.

Numerous studies show a broad variety of reasons for tumor initiation, including gene amplification, cellular stress, metabolic alteration, and epigenetic changes. This work suggests that the disruption of the cell competitive process mediated by secretory miRNAs will result in the occurrence of neoplasm. Understanding the mechanism by which homeostasis is impaired leads to a novel therapeutic approach for cancer progression.

Acknowledgments—We thank Katsuyuki Hayashi and Ikuei Hiraka at DNA Chip Research Inc. for supporting the processing of microarray data. We thank Ayako Inoue for excellent technical assistance.

REFERENCES

1. Johnston, L. A. (2009) Competitive interactions between cells: death, growth, and geography. *Science* **324,** 1679–1682
2. Díaz, B., and Moreno, E. (2005) The competitive nature of cells. *Exp. Cell Res.* **306,** 317–322
3. Hanahan, D., and Weinberg, R. A. (2011) Hallmarks of cancer. The next generation. *Cell* **144,** 646–674
4. Bondar, T., and Medzhitov, R. (2010) p53-mediated hematopoietic stem and progenitor cell competition. *Cell Stem Cell* **6,** 309–322
5. Dong-Le Bourhis, X., Berthois, Y., Millot, G., Degeorges, A., Sylvi, M., Martin, P. M., and Calvo, F. (1997) Effect of stromal and epithelial cells derived from normal and timorous breast tissue on the proliferation of human breast cancer cell lines in co-culture. *Int. J. Cancer* **71,** 42–48
6. Senoo-Matsuda, N., and Johnston, L. A. (2007) Soluble factors mediate competitive and cooperative interactions between cells expressing different levels of *Drosophila* Myc. *Proc. Natl. Acad. Sci. U.S.A.* **104,** 18543–18548
7. Kosaka, N., Iguchi, H., Yoshioka, Y., Takeshita, F., Matsuki, Y., and Ochiya, T. (2010) Secretory mechanisms and intercellular transfer of microRNAs in living cells. *J. Biol. Chem.* **285,** 17442–17452
8. Croce, C. M. (2009) Causes and consequences of microRNA dysregulation in cancer. *Nat. Rev. Genet.* **10,** 704–714
9. Suzuki, H. I., Yamagata, K., Sugimoto, K., Iwamoto, T., Kato, S., and Miyazono, K. (2009) Modulation of microRNA processing by p53. *Nature* **460,** 529–533
10. Takeshita, F., Patrawala, L., Osaki, M., Takahashi, R. U., Yamamoto, Y., Kosaka, N., Kawamata, M., Kelnar, K., Bader, A. G., Brown, D., and Ochiya, T. (2010) Systemic delivery of synthetic microRNA-16 inhibits the growth of metastatic prostate tumors via down-regulation of multiple cell-cycle genes. *Mol. Ther.* **18,** 181–187
11. Peng, X., Guo, W., Liu, T., Wang, X., Tu, X., Xiong, D., Chen, S., Lai, Y., Du, H., Chen, G., Liu, G., Tang, Y., Huang, S., and Zou, X. (2011) Identification of miRs-143 and -145 that is associated with bone metastasis of prostate cancer and involved in the regulation of EMT. *PLoS One* **6,** e20341
12. Franses, J. W., Baker, A. B., Chitalia, V. C., and Edelman, E. R. (2011) *Sci. Transl. Med.* **3,** 66ra65
13. Savina, A., Vidal, M., and Colombo, M. I. (2002) The exosome pathway in K562 cells by Rab11. *J. Cell Sci.* **115,** 2505–2515
14. Trajkovic, K., Hsu, C., Chiantia, S., Rajendran, L., Wenzel, D., Wieland, F., Schwille, P., Brügger, B., and Simons, M. (2008) Ceramide triggers budding of exosome vesicles into multivesicular endosomes. *Science* **319,** 1244–1247
15. Gandellini, P., Folini, M., Longoni, N., Pennati, M., Binda, M., Colecchia, M., Salvioni, R., Supino, R., Moretti, R., Limonta, P., Valdagni, R., Daidone, M. G., and Zaffaroni, N. (2009) miR-205 exerts tumor-suppressive functions in human prostate through down-regulation of protein kinase Cepsilon. *Cancer Res.* **69,** 2287–2295
16. Clapé, C., Fritz, V., Henriquet, C., Apparailly, F., Fernandez, P. L., Iborra, F., Avancès, C., Villalba, M., Culine, S., and Fajas, L. (2009) miR-143 interferes with ERK5 signaling and abrogates prostate cancer progression in mice. *PLoS One* **4,** e7542
17. Kong, D., Li, Y., Wang, Z., Banerjee, S., Ahmad, A., Kim, H. R., and Sarkar, F. H. (2009) miR-200 regulates PDGF-D-mediated epithelial-mesenchymal transition, adhesion, and invasion of prostate cancer cells. *Stem Cells* **27,** 1712–1721
18. Fujita, Y., Kojima, K., Ohhashi, R., Hamada, N., Nozawa, Y., Kitamoto, A., Sato, A., Kondo, S., Kojima, T., Deguchi, T., and Ito, M. (2010) MiR-148a attenuates paclitaxel resistance of hormone-refractory, drug-resistant prostate cancer PC3 cells by regulating MSK1 expression. *J. Biol. Chem.* **285,** 19076–19084
19. Saito, Y., Friedman, J. M., Chihara, Y., Egger, G., Chuang, J. C., and Liang, G. (2009) Epigenetic therapy up-regulates the tumor suppressor microRNA-126 and its host gene EGFL7 in human cancer cells. *Biochem. Biophys. Res. Commun.* **379,** 726–731
20. Rauhala, H. E., Jalava, S. E., Isotalo, J., Bracken, H., Lehmusvaara, S., Tammela, T. L., Oja, H., and Visakorpi, T. (2010) miR-193b is an epigenetically regulated putative tumor suppressor in prostate cancer. *Int. J. Cancer* **127,** 1363–1372
21. Xu, B., Niu, X., Zhang, X., Tao, J., Wu, D., Wang, Z., Li, P., Zhang, W., Wu, H., Feng, N., Wang, Z., Hua, L., and Wang, X. (2011) miR-143 decreases prostate cancer cells proliferation and migration and enhances their sensitivity to docetaxel through suppression of KRAS. *Mol. Cell Biochem.* **350,** 207–213
22. Gibbings, D. J., Ciaudo, C., Erhardt, M., and Voinnet, O. (2009) Multivesicular bodies associate with components of miRNA effector complexes and modulate miRNA activity. *Nat. Cell Biol.* **11,** 1143–1149
23. Pegtel, D. M., Cosmopoulos, K., Thorley-Lawson, D. A., van Eijndhoven, M. A., Hopmans, E. S., Lindenberg, J. L., de Gruijl, T. D., Würdinger, T., and Middeldorp, J. M. (2010) Functional delivery of viral miRNAs via exosomes. *Proc. Natl. Acad. Sci. U.S.A.* **107,** 6328–6333
24. Miyanishi, M., Tada, K., Koike, M., Uchiyama, Y., Kitamura, T., and Nagata, S. (2007) Identification of Tim4 as a phosphatidylserine receptor. *Nature* **450,** 435–439
25. Kwak, P. B., Iwasaki, S., and Tomari, Y. (2010) The microRNA pathway and cancer. *Cancer Sci.* **101,** 2309–2315
26. Yu, X., Harris, S. L., and Levine, A. J. (2006) The regulation of exosome secretion. A novel function of the p53 protein. *Cancer Res.* **66,** 4795–4801

Yamamoto *et al. Molecular Cancer* 2011, **10**:135
http://www.molecular-cancer.com/content/10/1/135

MOLECULAR CANCER

RESEARCH Open Access

An integrative genomic analysis revealed the relevance of microRNA and gene expression for drug-resistance in human breast cancer cells

Yusuke Yamamoto[1,2,4], Yusuke Yoshioka[1,2,4], Kaho Minoura[3], Ryou-u Takahashi[1], Fumitaka Takeshita[1], Toshiki Taya[3], Reiko Horii[3], Yayoi Fukuoka[3], Takashi Kato[2], Nobuyoshi Kosaka[1] and Takahiro Ochiya[1*]

Abstract

Background: Acquisition of drug-resistance in cancer has led to treatment failure, however, their mechanisms have not been clarified yet. Recent observations indicated that aberrant expressed microRNA (miRNA) caused by chromosomal alterations play a critical role in the initiation and progression of cancer. Here, we performed an integrated genomic analysis combined with array-based comparative hybridization, miRNA, and gene expression microarray to elucidate the mechanism of drug-resistance.

Results: Through genomic approaches in MCF7-ADR; a drug-resistant breast cancer cell line, our results reflect the unique features of drug-resistance, including MDR1 overexpression via genomic amplification and miRNA-mediated TP53INP1 down-regulation. Using a gain of function study with 12 miRNAs whose expressions were down-regulated and genome regions were deleted, we show that miR-505 is a novel tumor suppressive miRNA and inhibits cell proliferation by inducing apoptosis. We also find that Akt3, correlate inversely with miR-505, modulates drug sensitivity in MCF7-ADR.

Conclusion: These findings indicate that various genes and miRNAs orchestrate to temper the drug-resistance in cancer cells, and thus acquisition of drug-resistance is intricately controlled by genomic status, gene and miRNA expression changes.

Keywords: aCGH, microRNA, gene expression, breast cancer, drug resistance

Background

Systemic therapy improves disease-free survival in patients with breast cancer, but does not cure patients with advanced or metastatic disease, and fails to benefit the majority of patients with localized breast cancer. Intrinsic resistance to chemotherapy is emerging as a significant cause of treatment failure, and evolving research has identified several potential causes of resistance [1]. For instance, P-glycoprotein (Pgp), the drug efflux pump encoded by the MDR-1 gene is associated with multidrug resistance in several kinds of advanced cancer. Furthermore, the multidrug resistance-associated protein MRP1 [2,3], breast cancer resistance protein (ABCG2) and other transporters [4], which act as energy-dependent efflux pumps capable of expelling a large range of xenobiotics, have been reported to be upregulated in tumor cells showing the multidrug-resistant phenotype. In addition, overexpression of anti-apoptotic proteins, such as Bcl-2 and Bcl-xL, are also associated with drug resistance and poor clinical outcome in cancer patients. It is essential to decide the molecular target to treat the advanced cancer by molecular targeted therapies such as RNA interference and antibody treatment, however, regulatory networks underlying drug resistance in cancer cells have been elusive.

MicroRNAs (miRNAs) are small non-coding RNA of 21-25nt transcripts, playing central roles in physiological and pathological processes, including cell differentiation, apoptosis, and oncogenesis by either inducing mRNA degradation or by regulating the translational efficiency of mRNA [5-7]. Recently, several research groups have

* Correspondence: tochiya@ncc.go.jp
[1]Division of Molecular and Cellular Medicine, National Cancer Center Research Institute, 1-1, Tsukiji, 5-chome, Chuo-ku, Tokyo 104-0045, Japan
Full list of author information is available at the end of the article

provided evidence that some miRNA expression levels are frequently modulated by genomic aberrations, such as genomic DNA copy number gain or loss, translocations, and epigenetic regulations [8]. For example, miR-15a and miR-16-1, whose genomic regions are deleted and expressions are down-regulated in the majority of chronic lymphocytic leukemia (CLL). Furthermore, their target Bcl-2 is overexpressed in CLL at the mRNA and protein level [9]. Another study showed that the expression level of miR-34a was down-regulated by deletion of 1p36 heterozygosity in neuroblastoma and contributed to an aggressive phenotype [10]. As reported in the studies of cancer genetics in lung, leukemia, colon, breast and ovary, a large number of miRNAs are located at chromosomal fragile sites, i.e., minimal regions of loss of heterozygosity (LOH) and minimal regions of genomic amplification [11]. These reports indicated that the emphasis on a genomic analysis was due to the fact that DNA copy number alterations are associated with expression levels of miRNAs and genes.

In this study, to better understand the regulatory network underlying drug resistance in breast cancer cells, we focus on miRNAs and genes located on the genome-amplified and -deleted regions because genomic aberration is closely associated with gene expression, and this expression alteration might be constantly maintained. For the identification of molecular targets, we initially performed an integrated genomic analysis to compare the DNA copy number and expression profile of mRNA and miRNA between MCF7; a parental breast cancer cell line and MCF7-ADR; a drug-resistant breast cancer cell line [12,13]. Through the genomic analysis, we found that the genomic alterations of drug resistance-related genes, e.g. amplified genomic regions and overexpression of MDR-1 and miRNA-mediated TP53INP1 down-regulation. In addition, of 12 miRNAs whose expressions were down-regulated and genomic regions were deleted, we determined that miR-505 promotes the inhibition of cell growth in MCF7-ADR cells, by inducing apoptotic cell death in the presence of docetaxel (DOC).

Methods

Cell culture

MCF7 human mammary carcinoma cells and multidrug-resistant MCF7-ADR human mammary carcinoma cells were obtained from Shien-Lab, Medical Oncology, National Cancer Center Hospital. MCF7-ADR-Luc cells were established by transfecting with a pLuc-neo expression vector, which has the firefly luciferase GL3 cDNA cloned into the downstream of the SV40 promoter and the G418 selective marker gene. Cells were selected in a medium containing 0.6 mg/ml of G418 (Gibco BRL) and were maintained and passaged in an RPMI 1640 medium (Gibco BRL) supplemented with 10% fetal bovine serum (Gibco BRL) under 5% CO_2 in a humidified incubator at 37°C.

RNA and genomic DNA extraction

Total RNA was extracted from MCF7, MCF7-ADR, and MCF7-ADR-Luc cells using the ISOGEN solution (Nippon Gene, Tokyo, Japan) according to the manufacturer's protocol. Genomic DNA was prepared from MCF7 and MCF7-ADR. The yield and purity of the genomic DNA and total RNA were measured using a NanoDrop ND-1000 spectrophotometer (Thermo Fisher Scientific). The quality of the total RNA was verified to have an RNA Integrity Number using a Bioanalyzer and RNA 6000 LabChip Kit (Agilent Technologies).

Oligonucleotide array CGH (aCGH) Analysis

All DNA labeling reactions and hybridizations were carried out following the manufacture's protocol (Agilent Oligonucleotide Array-Based CGH for Genomic DNA Analysis, Version 4.0, Direct Method). Briefly, 3.0 μg of MCF-7, MCF7-ADR and reference DNA (Promega, female, p/n G1521) were digested with *Alu*I and *Rsa*I for 2 hours at 37°C, followed by heat inactivation at 65°C for 10 minutes. Digested DNA was then labeled using the Agilent Genomic DNA Labeling Kit Plus (p/n 5188-5309) using random primers and the exo-Klenow fragment to differentially label genomic DNA samples with fluorescently labeled nucleotides. All experimental and reference samples were labeled with Cyanine-5 dUTP and Cyanine-3 dUTP, separately, for 2 hours at 37°C to enable duplicate hybridizations with the corresponding dye reversal arrays. Experimental and reference targets for each hybridization were purified with a Microcon YM-30 column (Millipore) and validated by the NanoDrop ND-1000, respectively to ensure the yield and the specific dye incorporation activity of the labeled genomic DNA. The individual pair of labeled targets were combined together, mixed with Cot-1 DNA (Invitrogen) and 10xBlocking Agent (Agilent), and then mixed with Agilent 2xHybridization Buffer (p/n 5188-5220). Before hybridization, the combined mixtures were denatured for 3 minutes at 95°C, incubated for 30 minutes at 37°C and then applied to the Agilent Human 244A CGH arrays (G4411B). Using an Agilent microarray hybridization chambers, the hybridization was carried out for 40 hours at 65°C in a rotating oven (Agilent) at 20 r.p.m. The hybridization chambers were then disassembled and array slides were washed for 5 minutes at room temperature in Agilent Oligo aCGH Wash Buffers 1, followed by 1 minute at 37°C in Agilent Oligo aCGH Wash Buffer 2 (p/n 5188-5226) (prewarmed to 37°C overnight). The slides were removed from the wash buffer 2 slowly (5-10 seconds) after which time they were completely dry and were scanned using an Agilent DNA Microarray scanner with 5 μm resolution. The data of microarray

images were extracted by Agilent Feature Extraction Software v9.5 in which a modified Feature Extraction protocol, CGH-v4_95_Feb07 was used in conjunction with a gene list on chromosome 21 q-arm to normalize spot-intensity values and ratios to each extraction set. These ratio data along with associated error values and flagged features were imported into CGH Analytics Software v3.4 (Agilent). The dye reversal data and intra-replicate spots were then combined while the data centralization and fuzzy zero algorithms were not applied in the CGH Analytics. To make aberration calls, an aberration detection algorithm, ADM-2 [14] was used at threshold 10 and an aberration filter was set at 2 for the minimum number of probe region and 1 for minimum absolute average log2 ratio for regions in the CGH Analytics to reduce false positives.

Gene Expression Analysis

All RNA labeling reactions and hybridizations were carried out following the manufacture's protocol (Agilent One-Color Microarray-Based Gene Expression Analysis, Version 5.0.1). Briefly, polyA(+)RNA in 500 ng of total RNA was primed with an oligo (d)T-T7 primer and converted into dsDNA with MMLV-RT, then transcribed and simultaneously labeled with Cyanine 3-CTP for 2 hours at 40°C using Agilent Low RNA Input Linear Amplification Kit (p/n 5188-5339). After labeling and cRNA purification, cRNA was quantified and the specific dye incorporation activity was validated using the NanoDrop ND-1000. 1.65 μg of labeled cRNA was mixed with Agilent 10×Blocking Agent and 25×Fragmentation Buffer, then incubated at 60°C for 30 hours. After fragmentation, the cRNA mixtures were immediately mixed with Agilent 2×Hybridization Buffer (p/n 5188-5339) and applied to the Agilent Human 4×44 K whole genome microarrays (G4112F) for 17 hours at 65°C (10 r.p.m.). Array slides were washed with Agilent Gene Expression Wash Buffer 1 and 2 (p/n 5188-5327) and then scanned using the Agilent DNA Microarray scanner with 5 μm resolution and the eXtended Dynamic range setting (XDR Hi 100%, Low 10%) to avoid saturated features. The data of microarray images were extracted by Agilent Feature Extraction Software v9.5 using the GE1_v5_95 protocol. The extracted signal intensities and flagged information were imported into GeneSpring 7.3.1 software and the data sets were normalized by adjusting the intensity distribution of well-above background and unflagged features to 50th percentile to account for the interchip variability. Comparison of MCF7 and MCF7-ADR was done using duplicate array data set for each cell line.

miRNA Expression Analysis

All RNA labeling reactions and hybridizations were carried out following the manufacture's prototype protocol (Agilent miRNA Microarray system, Version 0.3, early access). Briefly, 100 ng of total RNA including fraction of small mature miRNA was dephosphorylated by calf intestine alkaline phosphatase (p/n E2250Y, Amersham Biosciences) for 30 minutes at 37°C and denatured by adding DMSO (p/n D8418, Sigma) for 8 minutes at 100°C. Ligation was then carried out with T4 RNA ligase (p/n E2050Y, Amersham Biosciences) and pCp-Cy3 (p/n 5190-0408, Agilent) for 2 hours at 16°C that allowed us to perform a quantitative direct labeling method [15]. The labeled miRNAs were desalted with Micro Bio-Spin 6 column (p/n 732-6221, Bio-Rad) and combined with Agilent 10×GE Blocking Agent and 2×Hybridization Buffer (p/n 5190-0408). The mixture was heated for 5 minutes at 100°C and immediately cooled to 0°C. Each sample was hybridized to the Agilent early access Human 8×15 K microRNA microarrays covered 470 miRNAs (AMADID 015508, early access) for 20 hours at 55°C (20 r.p.m.). Array slides were washed with 6× SSC/0.005% Triton X-100 for 10 minutes, then 0.1× SSC/0.005% Triton X-100 for 5 minutes, both at room temperature. Slides were scanned using the Agilent DNA Microarray scanner with 5 μm resolution and the eXtended Dynamic range setting (XDR Hi 100%, Low 5%) to avoid saturated features. The data were extracted by Agilent Feature Extraction Software v9.5 using the miRNA_120106 protocol which extracts intensities of multiple probes with multiple features per probe and reports the measurements and errors as the TotalGeneSignal and TotalGeneSignalError for each of the miRNAs. These values were imported to the GeneSpring GX version 7.3.1 without applying any normalization algorithm. The miRNA profiles generated on the Agilent platform were prior normalized to the amount of input total RNA in which 100 ng of total RNA were equally used for each assay and all of the labeled targets were loaded on each array. Comparison of MCF7 and MCF7-ADR was done using duplicate array data set for each cell line.

Transfection of miRNA into MCF7-ADR-Luc cells

For MCF7-ADR-Luc cells, transfection of miRNA was carried out using DharmaFECT 1 (Dharmacon) according to the manufacturer's protocol. MCF7-ADR-Luc cells were plated in growth medium 24 hours before transfection. The cells, which were grown to 50% confluence, were transfected with 20 nM miRNAs and cultured. Two or 3 days after transfection, the cells were subjected to further analyses.

Apoptosis assay measurement of caspase activity *in vitro*

Caspase-7, which plays key effecter roles in apoptosis, was detected in caspase-3-deficient MCF7-ADR-Luc cells. The arrays used in an *in vitro* growth assay were

measured with the Apo-ONE Homogeneous Caspase-3/7 Assay (Promega) according to the manufacturer's instructions. Cells were incubated with the Apo-ONE Caspase-3/7 Assay Reagent for 1.5 hours at room temperature, and the fluorescence was then measured at 485Ex/535Em with a Wallac Multi-label Counter.

Hoechst staining

Cells were washed with PBS(-), and a fixative and staining solution was added (4% paraformaldehyde, 1 μg/ml Hoechst 33342 in PBS). Ten minutes after incubation, cells were washed with PBS, and the number of apoptotic cells was then determined in three microscopic fields of each well by fluorescence microscopy (Olympus).

Luciferase assay for the measurement of cell growth

MCF7-ADR-Luc cells were plated into 5×10^3 cells per well and cultured. The cell growth in each well was then estimated by firefly luciferase activity because the cell numbers were correlated with the bioluminescence from MCF7-ADR-Luc cells. Luciferase assays were performed with a Wallac Multi-label Counter (PerkinElmer) and Bright-Glo Luciferase Assay System (Promega, Tokyo, Japan) according to the manufacturer's protocol.

Real-time RT-PCR

The total RNA was used to produce cDNAs with the SuperScript™ II First-Strand Synthesis System (Invitrogen, Tokyo, Japan) according to the manufacturer's protocol. For quantification, cDNA samples were subjected to real-time PCR using Platinum SYBR Green qPCR SuperMix UDG (Invitrogen) in triplicates, and reactions were carried out in an ABI PRISM 7300 (Applied Biosystems, Tokyo, Japan). The specific sequences of primers for the analyzed genes are shown in Additional File 1 Table S1. The expression levels of genes were normalized to GAPDH. For miRNA real-time RT-PCR, total RNAs of approximately 100 ng were reverse-transcribed using the Taqman miRNA reverse transcription kit (Applied Biosystems). Real-time quantitative PCR amplification of the cDNA template was done using Taqman Universal PCR Master Mix (Applied Biosystems, Tokyo, Japan) in an ABI PRISM 7300 (Applied Biosystems). The PCR conditions were 50°C for 2 minutes and 95°C for 10 minutes followed by 50 cycles of 95°C for 15 seconds and 60°C for 1 minute. Taqman probes for human were used to assess the expression levels of miRNAs (hsa-miR-505, ID: 4373230, hsa-miR-130, ID: 000454, and hsa-miR-155, ID: 002623).

3'UTR assay plasmid constructs

A 1235 bp fragment from the 3'UTR of Akt3 containing the predicted target sequence of miR-505 (located at positions 529-535 of the Akt3 3'UTR) and a 934 bp fragment from the 3'UTR of Akt3 containing the predicted target sequence of miR-505 (located at positions 529-535 of this fragment) were PCR-cloned from MCF7-ADR cells isolated total RNA. Three prime A-overhang was added to the PCR products after 15 minutes of regular Taq polymerase treatment at 72°C. The PCR products were cloned into a pGEM-T easy vector (Promega). The amplified products were ligated into the NotI sites of the 3'UTR of the *Renilla* luciferase gene in the psi-check-2 plasmid (Promega) to generate psi-Akt3_1 (1235 bp) and psi-Akt3_2 (934 bp). Primer sequences used for PCR-cloning were shown as below: Akt3_F, GAGCCAGAGAGCATCT TTCC, Akt3_R1, GCTGCCTTAGTAAAATGCCC, and Akt3_R2, GACTTCACAGGCTGCTTTGG.

Statistical analysis

The results are given as the mean ± s.d. Statistical analysis was conducted using the analysis of variance with the Student's t-test. A P value of 0.05 or less was considered to indicate a significant difference.

Results

An integrated genomic analysis unveils the status of cancer cells

MCF7-ADR is a multi-drug resistant cell line derived from MCF7 breast cancer cell line. We utilized these two cell lines to understand the regulatory network underlying drug resistance in breast cancer and conducted three types of genomic analysis, i.e. array-based comparative hybridization (aCGH) (Figure 1B), miRNA (Additional File 2 Figure. S1A) and gene expression (Additional File 2 Figure. S1B). Genes and miRNAs, which are located on the genome-amplified and -deleted regions, are expected to be responsible for drug resistance and sensitivity. Moreover, these three types of array data were used for miRNA target prediction and pathway to further elucidate key factors for drug resistance (Figure 1A).

As a consequence of array-based CGH, changes in DNA copy number in MCF7-ADR and MCF7 as compared with normal female genome were found in a large number of regions as amplification and deletion (Figure 1B). Accuracy of array-based CGH was validated by dye flip experiment that exhibited strikingly mirroring images (Additional File 3 Figure. S2). The numbers of genes and miRNAs located on the amplified and deleted genome regions (fold change > 3) in MCF7-ADR and MCF7 cells are shown (Figure 1C). On further comparison, a large number of changes in gene and miRNA expressions were observed between MCF7 and MCF7-ADR (Additional File 2 Figure. S1A and B). These genes with aberrant differences were observed predominantly in amplified region in MCF7 and, in contrast, they were mainly in deleted regions in MCF7-ADR (Figure 1B and 1C). In a different criterion of aCGH data (fold change > 2), we could see the same propensity more clearly (Additional File 4 Figure. S3A and B).

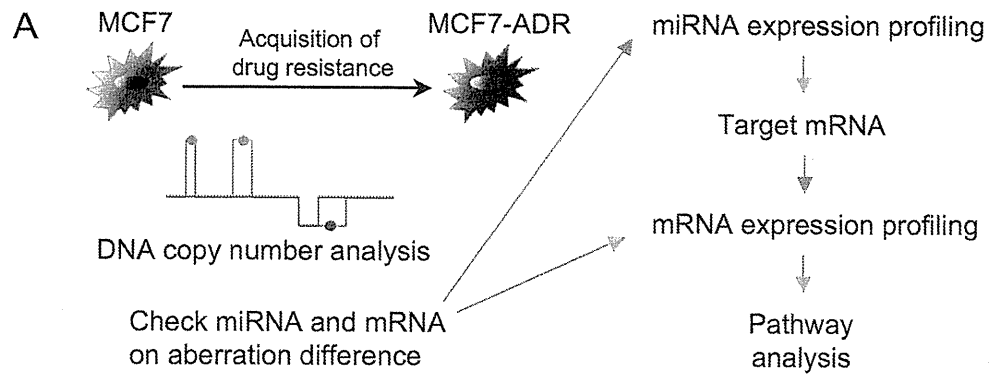

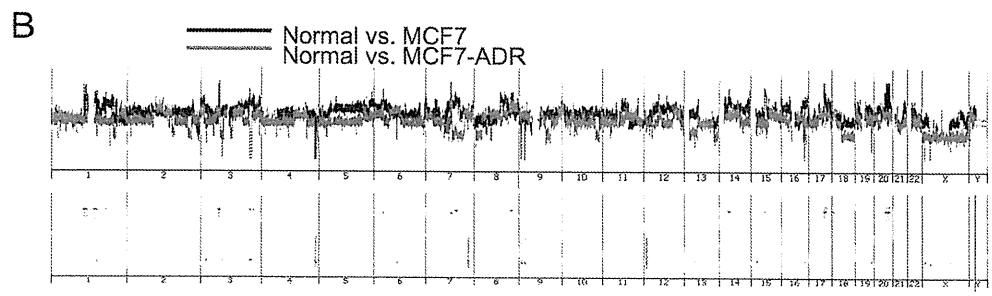

C

DNA copy Number	MCF7		MCF7-ADR		
	Gene	miRNA	Gene	miRNA	
Amp	426	7	6	0	
Del	6	0	25	1	FC > 3

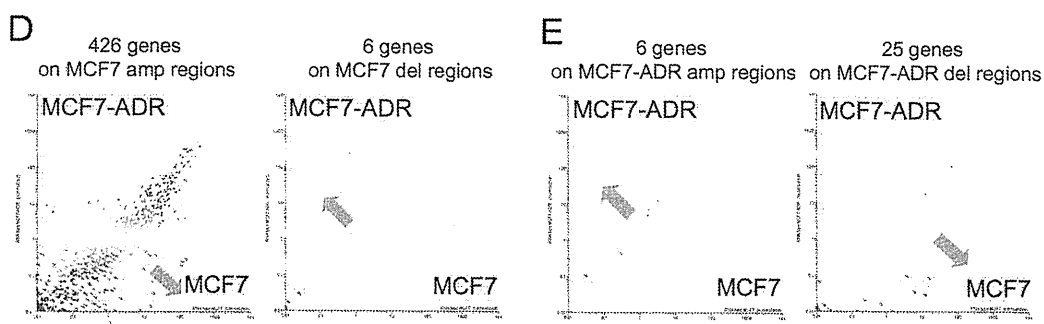

Figure 1 An integrated genomic analysis to clarify drug resistance in MCF7-ADR (drug-resistant breast cancer cell line). (A) Schematic representation of an integrated genomic analysis. During the acquisition of drug resistance in breast cancer cell (MCF7; parental cell line and MCF7-ADR; drug resistance cell line), a large number of genomic alterations were raised, such as amplification or deletion, to modulate the expression of genes and miRNAs. Based on aCGH, miRNAs and genes on the aberration region of genome are selected for further analysis of its target genes and their associated-pathways *in silico*. (B) aCGH analysis of MCF7 and MCF7-ADR as compared with normal human female genome. Blue line shows normal vs. MCF7, and red line shows normal vs. MCF7-ADR (top). Amplified or deleted genome regions (fold change > 3) are highlighted (bottom). (C) The numbers of genes and miRNAs located on the amplified or deleted genome regions (FC > 3). (D and E) The expression tendency of genes located on the aberrant genome regions. 426 genes from MCF7 amplified regions and 6 genes from MCF7-ADR amplified regions are plotted in left panels of each scatter plot. Six genes from MCF7 deleted regions and 25 genes from MCF7-ADR deleted regions are plotted in right panels of each scatter plot.

Because genomic amplification and deletion are thought to be associated with up- and down-regulation in expression, respectively, 426 genes on the amplified region in MCF7 and 6 genes on the deleted regions in MCF7 were plotted (Figure 1D). When the expression levels of amplified 426 genes and deleted 6 genes were checked, the expression of 426 genes tended to increase (Figure 1D left), and *vice versa* that of 6 genes tended to decrease in MCF7 as compared with MCF7-ADR (Figure 1D right), although these gene numbers were counted based on the comparison of MCF7 and normal female genome. Consistent with MCF7 result, we can see similar tendency in gene expression in the result of MCF7-ADR (Figure 1E), indicating that the gene expression levels and genomic alterations are broadly correlated in this experiment.

An integrated genomic analysis reflects the unique features of drug resistance in breast cancer cells

We hypothesized that genes and miRNAs in the region of genomic alteration were relevant to drug resistance in MCF7-ADR cells. In the most amplified region in MCF7-ADR, we found MDR1 gene, which is an important efflux pump for drug resistance. Its genome locus was amplified more than 20-fold (Figure 2A), and its expression was up-regulated 800-fold or more in MCF7-ADR by microarray (Figure 2B). Expression level of MDR1 was confirmed by real-time RT-PCR and was observed to be remarkably up-regulated in MCF7-ADR consistent with our previous study (Figure 2C) [13], suggesting that the genomic amplification and overexpression of MDR1 were one of the reasons for drug resistance of MCF7-ADR.

Next, we tried to know the target genes of differentially-expressed miRNA in MCF7-ADR, because these genes might act as key molecules for drug resistance. Seventy-four miRNAs were 2 fold or more up-regulated in MCF7-ADR (Figure 3A), and we selected genes that have binding sites of more than 15% of up-regulated miRNAs in their 3'UTR. The scatter plot shows expression levels of these genes (Figure 2D), and 3 gene names are displayed because their expression levels are considerably down-regulated in MCF7-ADR. One of them is tumor protein p53 inducible nuclear protein 1 (TP53INP1) (Figure 2D), which has been recently shown to be suppressed by several miRNAs such as miR-130 and miR-155 [16,17]. Furthermore, decreased expression of TP53INP1 is involved in breast cancer progression [18]. As shown in Figure 2E, expression of miRNAs which potentially bind to 3'UTR of TP53INP1 were plotted, and it displays names of miRNAs whose expression levels were considerably up-regulated in MCF7-ADR. These included miR-130 and miR-155 also known as TP53INP1 binding miRNAs, and most of them are highly expressed in MCF7-ADR, indicating that these miRNAs and TP53INP1 expressions were inversely correlated. From the real-time RT-PCR analysis, down-regulation of TP53INP1 and up-regulation of miR-130 and miR-155 in MCF7-ADR as compared with MCF-7 (Figure 2F and 2G). Taken together with our results and recent publications, our integrated genomic analysis can clearly reflect the status of multi-drug resistant MCF7-ADR.

Pathway analysis of up- and down-regulated miRNA target genes

Cancer cells abrogate the function of drug sensitive genes, such as tumor suppressor gene and related-gene pathway after the anticancer drug treatment, and thus we speculated that differentially-expressed miRNAs between MCF7-ADR and MCF7 controlled the gene pathway governing drug resistance. As shown in Figure 3A, 74 miRNAs and 32 miRNAs were up- and down-regulated in MCF7-ADR, respectively. Target gene prediction showed up-regulated 74 miRNAs had 5, 137 genes and down-regulated 32 miRNAs had 3, 579 genes as target candidates (Figure 3A). Expression levels of these genes were plotted in the scatter plots, however, decreasing and increasing expression tendencies were not clearly observed (data not shown). So, with these genes, we next checked what kind of gene pathways were expected to be regulated by differentially-expressed miRNAs. A large number of pathways were significantly chosen (Top 20 pathways shown in Additional File 5 Table S2). Surprisingly, many common pathways were enriched in both up-and down-regulated miRNA targeted genes, suggesting that the differentially-expressed miRNAs orchestrated to lead the global gene expression changes in MCF7-ADR. Intriguingly, these miRNAs seem to regulate some of drug resistance related signaling pathways, such as Wnt, insulin, EGFR1, MAPK and TGF-beta receptor (Additional File 5 Table S2, Figure. 3B and Additional File 6 Figure. S4). This data shows the possibility that differentially-expressed miRNAs might cooperatively regulate their target pathways and change drug resistance and sensitivity in MCF7-ADR.

Identification of miRNAs that suppress cell proliferation in MCF7-ADR

We next explored whether the miRNAs that were located on the aberrant genome regions played a role in regulating drug resistance of MCF7-ADR. To this end, genomic status between MCF7-ADR and MCF7 were directly compared (Figure 4A). The numbers of genes and miRNAs that were located on the aberrant regions are shown (Figure 4B) and most of them were on the deleted regions in MCF7-ADR. A scatter plot showed 49 miRNAs on the deleted genomic regions in MCF7-ADR (Figure 4C) and expression levels of these 49 miRNAs had decreasing trend in MCF7-ADR. In this study, we focus on miRNAs whose expressions were down-regulated and genomic